Improving CO_2 gas barrier properties of polymer-based membranes in gas pipelines using 2D nanosheets

By

Abubakar Sudais

School of Chemical & Materials Engineering

National University of Sciences & Technology

June 2022

Improving CO_2 gas barrier properties of polymer-based membranes in gas pipelines using 2D nanosheets

Name: Abubakar sudais

Reg. No: 00000320585

This thesis is submitted as the partial fulfillment of the requirements of the degree of

MS in Chemical Engineering

Supervisor Name: Dr. Sarah Farrukh

School of Chemical and Materials Engineering (SCME)

National University of Sciences and Technology (NUST)

H-12, Islamabad, Pakistan

June 2022

Dedication

I dedicate this work to my parents and without their unflinching support, it would not have been possible.

Acknowledgments

All praise belongs to Allah Almighty, the Most Benevolent and the Most Merciful, who has given me the ability and aptitude to complete this work.

I would like to thank **Dr. Sarah Farrukh** for her relentless support throughout this project. Her vision, resolve, and expertise made navigation through all the hurdles effortless. No matter how much I praise her it would still be an understatement of how much great a human being she is, and I feel extremely lucky to have been mentored by such an efficient and amiable personality. Her unwavering belief in my abilities made things much easier and for that, I'm eternally indebted to her.

I would like to express my gratitude to my GEC members **Dr. Tayyaba Noor** and **Dr. Aftab Akram** for their help and guidance in every step of the way.

Finally, I would like to thank all the friends for their immense moral support from beginning to the end, particularly during the troublesome circumstances when this project seemed too far-fetched.

Abstract

Industrial growth has played a vital role in facilitating human beings. Fossil fuels are widely used for different purposes. Several oil refineries and rigs are implanted comprising a huge pipeline network. Carbon steel is mostly used for pipes. Metal and corrosion always exist in parallel to each other, so corrosion of pipelines in fuel industries is a very highlighted problem. Advancement of materials and processes aids to solve industrial issues in a novel and smart method. 2D materials are incorporated with other polymers to form different new materials. Corrosion-resistant coatings are synthesized to increase the lifetime of pipelines. This study is done to produce PET (Polyethylene Terephthalate) films with MoS_2 (molybdenum disulfide) nanosheets as a filler on the laboratory scale. Thin films act as a coating to resist corrosion. Liquid phase exfoliation was applied for the synthesis of nanosheets. Temperature-induced phase separation (TIPS) was the approach employed to prepare PET/MoS_2 nanocomposites. Centrifuge RPM during the preparation of nanosheets and weight percent of filler in PET was variable to study the effect of these factors, other variables of the experiment were kept constant. Among 500, 1000, and 1500 RPMs, 500 rpm was titled as best on basis of gas barrier properties. Filler weight percentages of 0.0025, 0.005, and 0.01 were added to PET, 0.01 appeared to be the best percentage. Gas permeation tests proved the enhanced gas barrier properties of thin films. Experimental results were compared with theoretical models, and it was found that the Cussler model closely fits our experimental results. 95% reduction in permeation was achieved using only .00025wt% MoS_2 nanosheet filler. CO_2 gas was used for the permeation test, the duration of testing was 8 to 24 hours. SEM (Scanning Electron Microscopy), AFM (Atomic Force Microscopy) images of fillers and peaks through XRD (X-Ray Diffraction) authenticate successful synthesis of nanosheets. Same, SEM and XRD were performed for thin PET/MoS_2 films to study and verify the decrease in porosity and presence of MoS_2 nanosheets.

Table of Contents

List of Figures

List of Tables

List of Acronyms

MSNS Molybdenum disulfide nanosheets

PET Polyethylene Terephthalate

NMP N-methyl-2-Pyrollidone

DMT Di Methyl Terephthalate

OTR Oxygen Transmission Rate

TIPS Temperature Induced Phase Separation

Chapter 1 - Introduction

1.1 Background

Natural gas power plants are the most resourceful fossil fuel power plants in service today. [1] One of the most challenging matters is the transportation of these resources. Refined Natural gas requires pipelines for its transportation. Refined Natural gas contains 0.57% CO2 which results in corrosion in long-distance pipelines. [2] Failure in gas pipelines is not only due to corrosion, Incorrect operation, welding, material, equipment failure, and other causes are also factors in gas pipeline failures. However, the major parameter in gas pipeline failure is corrosion with the following reactions.

$CO_{2\,(aq)} + H_2O \quad \rightleftharpoons \quad H_2CO_3$

$Fe + CO_2 + H_2O \quad \rightarrow \quad Fe^{+2} + CO_3^{-2} + H_2O$

Generally, there are two main methods for the protection of corrosion.

I. Coating

- Fusion Bonded Epoxy
- 3- Layered polyethylene
- Coal tar
- Asphalt

II. Cathodic Protection

In such a method impressed current or sacrificial anode is used for corrosion prevention. Nowadays, researchers are finding much more effective coating materials to prevent corrosion. Conventionally 0D (silica nanoparticles), 1D (carbon nanotubes), and 3D (segregated graphene nanoplatelets) materials were used for different industrial applications such as electronics, sensors, biomedical, etc. But over the past decades, 2D materials got attention due to their marvelous properties of 2D nano-plane, bio compatibility, bio degradability, thermal conductivity, and gas barrier. [3, 4]. There are

different types of 2D materials such as graphene, molybdenum disulfide (MoS_2), tungsten disulfide, hexagonal boron nitride (h-BN), etc. The discovery of graphene in 2004 caught splendid attraction towards 2D materials due to its high thermal conductivity, protective coating, and gas barrier properties. Graphene is a single layer of graphite (the simplest allotropic form of carbon) having a hexagonal crystalline structure. It is used for a variety of applications in the field of electronics, sensors, biomedical, and membrane technology. [5, 6]. Although graphene exhibits extensive properties it does not show a bandgap (minimum energy needed for an electron to set free from its bound state) as compared to other 2D materials [7]. Commercially graphene has low production due to its high cost. The dispersibility and compatibility of graphene in polymers is poor. Hydrophobicity and agglomeration are the other two properties which bring graphene to lower priority among the other 2D materials. These 2D materials have plenty of uses with polymeric materials in different industries.

One of the most apparent effects of urbanization has been a shift of the industrial sector towards PET packaging, especially in the carbonated beverages sector, PET polymer consumption has been ample in bottle making and its market continues to grow such are its exceptional properties. In recent times for the above-mentioned application, traditional materials like metals (aluminum cans) and glass bottles have been substituted by PET polymer due to cost-effectiveness, easier processing, light weightiness, and unbreakable characteristics. The first patent for PET polymer preparation is held by J. Rex Whinfield and James T. Dickson of England, who claimed to have invented a synthetic polymer having valuable but unusual properties which could be used for making textile fibers and filaments [8]. After the first PET bottle patent [9], plastics production surged over the next 50 years from 15 million tons in 1964 to 311 million tons in 2014 and is expected to double again over the next 20 years, where plastic packaging represents 26% of the total volume of plastic used [10]. Just as there are plenty of advantages of PET, there is one noticeable flaw with PET bottles i.e., their finite gas permeability characteristics [11-13], packaged beverages with low gas and vapor permeation rates have longer shelf-life [14], and this inherent issue limits the application of PET for packaging in this context [15]. O2 barrier properties of PET are not sufficient enough to give a satisfactory shelf life unless kept at

refrigeration temperatures also CO2 levels in carbonated beverages drop with time as a result of permeation through the walls[16], which decreases the overall flavor[17].

Permeability reduction of gases can be used to extend the shelf life of carbonated beverages. International Society of Beverages Technologists defines the shelf life of beverages in terms of loss of CO2 with storage time corresponding to 17.5% loss of CO2 for soft drinks and 10% for beer. Evaluation of shelf life in the beverages industry is a very critical issue, in the carbonated soft drinks application, estimation of loss of carbon dioxide or the external oxygen entrance through the walls has been a challenging matter. The shelf life of a carbonated drink relies substantially on the resistance offered by the polymeric container walls to the gas molecules trying to diffuse through them. Furthermore, PET has been observed to be more permeable to oxygen than glass, which results in drinks becoming stalled due to oxidation. Carbon dioxide levels in the drinks reduce with time due to permeation through the walls, and if the level drops below 15% the drink becomes stale and gives a flat taste, degradation of taste in drinks is also associated with bottles transparency since they allow easy access to the sunlight which further aids the degradation process. Loss of 15% carbonation in 90 days is considered acceptable for a two-liter bottle, which confines its storage time to nine months, whereas, for a 250mL bottle, the storage time is far less i.e., 2-3 months [18].

1.2 Molybdenum disulfide

Molybdenum disulfide is one of the most significant materials due to its low cost, robustness, high abundance, and exceptional activity [19]. MoS_2 layered structure material has weak out-of-plane interactions and strong in-plane bonding, because of these two it shows tremendous chemical, mechanical and physical properties [20]. MoS_2 is used for cocatalysts to provide the best cost-effectivity and efficient hydrogen photocatalytic production because of unsaturated Sulphur (S) atoms along with the affinity to proton (H^+) in solution [21]. Owing to its high thermal and chemical resistance MoS_2 is used as a constituent of equipment that involves high-temperature applications. Its melting point is close to 2,375 °C.

Due to its good lubricating properties, MoS_2 is the most widely used 2D material, its high electrical and chemical resistivity aids its application in the cosmetic industry. The structure of molybdenum disulfide takes the form of a hexagonal plane of S atoms on either side of a hexagonal plane of Mo atoms. These planes pile on top of each other, with strong covalent bonds sandwiched between the Mo and S atoms, but weak van der Waals forcing holding layers together. van der Waal forces that make the separation of a single layer(exfoliation) feasible when subjected to ultrasonication, termed as MoS_2NS (Molybdenum disulfide Nanosheets). MoS_2NS have typically higher aspect ratios than Nanoclays.

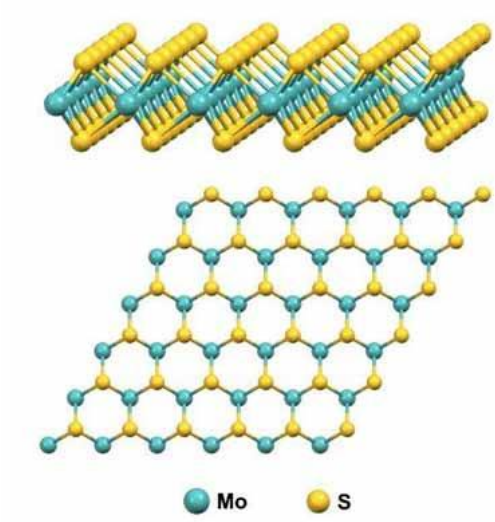

Figure 1: Molybdenum disulfide structure

1.3 Liquid Phase Exfoliation

Materials having a layered structure that exhibits strong in-plane covalent bonding and weak van der Waal bonding out of a plane can be separated into a single layer having a thickness in the nanometer range. This process of separating mono or few layers from their bulk precursor is termed as delamination or exfoliation, most popular method of exfoliating nanolayers is through the liquid phase exfoliation that involves using a solvent, liquid phase exfoliation is achieved through ultrasonication, it involves the transfer of high frequency sound wave energy to the liquid samples, when sonic energy is applied to the liquid sample, solvent molecules start to oscillate at the frequency of applied energy, during this process the sound waves go through compression and rarefaction cycles which causes the solvent

molecules to move towards and away from each other, during the rarefaction cycle solvent molecules move apart and exceed the critical molecular distance that keeps a liquid intact thereby generating cavities or bubbles, the cavities or bubbles formed collapse on the end of every rarefaction cycle releasing large amount of energy in the form of a shock wave, these wave generate high local shear stresses that result in the breakage of weak van der Waal forces and exfoliation of layers from the bulk. Since a considerable amount of energy is released during this process it is necessary to keep the sample cool by using a cooling bath.

1.4 PET (Polyethylene Terephthalate)

PET (also abbreviated PETE) is shorter than polyethylene terephthalate, a chemical name for polyester. PET is a clear, durable, lightweight plastic that is widely used for packaging food and beverages, especially soft drinks the size of juices, juices, and water. Almost all the simultaneous bottles of 2-liter cold drinks and carbonated water are sold in the U.S. made of PET. It is also famous for packing salad dressings, peanut butter, cooking oil, mouthwash, shampoo, liquid hand soap, window cleaner, and even tennis balls. Special PET tags used for home-grown food containers and prepared food trays can be heated in the oven or microwave. The basic properties of PET are ethylene glycol and terephthalic acid, which are synthesized to form a polymer chain. Fibers like PET spaghetti are extracted, cooled quickly, and cut into small pellets. The resin pellets are then heated in a melted liquid that can be easily extracted or molded into a material of any shape. Its crystallinity varies from amorphous to crystalline, thin pet films are transparent whereas thicker films have an opaque appearance. Since most variations of PET are semi-crystalline having a major crystalline portion its melting point (Tm) ranges between (250-260)oC, and so does its intrinsic viscosity which is also a measure of its molecular weight, bottle grade PET has IV ranging from (0.75-0.85)dL/g since it also contains amorphous regions, its glass transition temperature (Tg) depending upon the structure ranges from (67-81)oC

PET exhibits a semi-rigid to rigid structure depending on its thickness. PET Polyester fibers have been used in a wide variety of applications and the most of world's PET production is for synthetic fibers (over 60%) with bottle production accounting for around 30% of global need. In the late 1950s, PET was developed and used as a film in various applications

such as video, photographic, and X-ray films in addition to uses in flexible packaging. Later PET was modified and reinforced by micro fillers such as mica and glass which gave PET dimensional stability required for the use in injection molded and extruded materials. In the early 1970s PET was stretched by blow molding, stress blow molding techniques, and first oriented three-dimensional structures such as bottles were produced from the PET. This development was the cause of the rapid utilization of PET as a packaging material that is lightweight, tough, and chemically inert in addition to possessing moderately good gas barrier properties.

1.5 PET Manufacturing Processes

PET can be manufactured via two methods namely, esterification and transesterification former occurs between a carboxylic acid and alcohol whereas the latter involves a reaction between an ester and alcohol.

Esterification: This method (Figure 2) involves the direct esterification of Terephthalic acid with ethylene glycol, it's preferred over the transesterification process because of its high reaction rate, no catalyst requirement and results in higher molecular weight PET. Direct esterification is performed in the 220oC-260oC temperature range and (2.7-5.5) bar pressure range with water being continuously removed via distillation, the reaction could also be accelerated using amines if needed, gradual pressure along with temperature increase follows direct esterification in addition to the distillation of excess ethylene glycol, the next step is polycondensation that proceeds the same as in transesterification process.

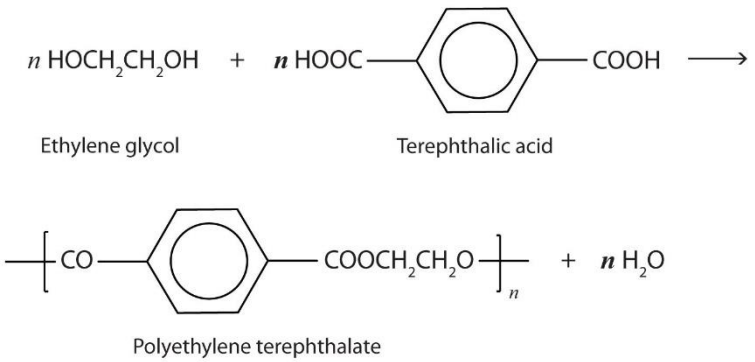

Figure 2: PET Manufacturing Process- Esterification

Transesterification: It is also called as DMT method (Figure 3), it involves the heating and melting along with stirring of DMT (Di-Methyl-Terephthalate) at 150-160oC in an inert environment containing nitrogen, heated DMT is then reacted, stirred, and heated at 150-200oC with ethylene glycol transesterification reactors at normal pressure under nitrogen atmosphere, the methanol produced is continuously removed via distillation which serves as a driving force for the reaction, the reaction occurs in the presence of basic catalysts namely metal oxides, amines, alkoxides, acetates, etc., with their concentration ranging from 0.01-0.1wt%. Product from transesterification reactors is transferred to a polycondensation reactor, and excess ethylene glycol from the previous reactor is distilled by a gradual increase in temperature to 250oC at normal pressure, followed by polycondensation that involves a reduction in pressure to <1bar and a rise in temperature to around 270oC-280oC for higher molecular weight polymer. This reaction to proceeds under the presence of catalysts, frequently used are germanium, antimony, lead compounds, and titanium at a miser concentration of 0.005-0.05wt%.

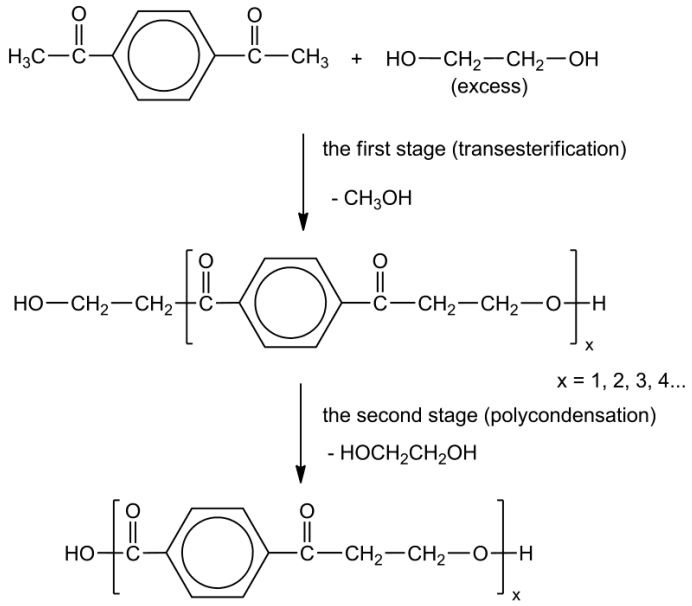

Figure 3: PET Manufacturing Process Transesterification

1.6 Need for MoS_2Ns-PET Nanocomposites

The high aspect ratio and biocompatible characteristics of MoS_2 nanosheets make them an ideal candidate for utilization in the gas pipeline industry where corrosion is a recurring issue. Considering their high aspect ratio, MoS_2 nanosheet incorporation into polymer would result in enhanced gas barrier properties without affecting other vital parameters, namely, chemical inertness and transparency. Polymer nanocomposites are a combination of polymer and nanofillers. This composite provides extensive properties which neat polymer cannot provide, like: Increase thermal resistance, enhance gas barrier properties, Improving mechanical properties, Simple processing ability, Enhancing the product value, and Light weight.

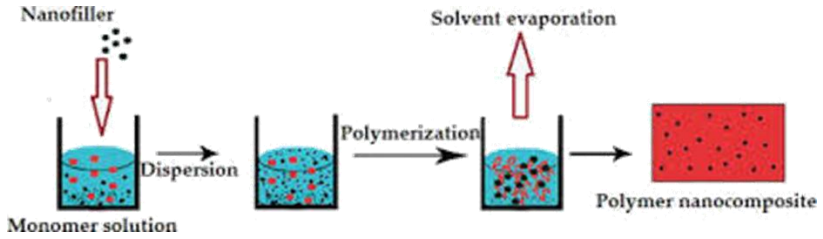

Figure 4: Polymer nanocomposites

Chapter 2 - Literature Review

In the past, materials like nano clays were used to affect the gas barrier properties. Enhancing gas barrier properties requires a high aspect ratio. Therefore, several 2D nanomaterials were used to enhance such properties. Graphene has got much attention to improve such properties due to its high aspect ratio. However, for some applications, graphene was not effective as it resists the material's transparency. Therefore, researchers are now moving to other 2D materials which are likely to be graphene. Hexagonal boron nitride, molybdenum disulfide, and tungsten disulfide are the new 2D materials like graphene. So such nanomaterials incorporated with polymers are very effective in the enhancement of gas barrier properties. Molybdenum disulfide (MoS_2) is one of the most significant materials due to its low cost, robustness, high abundance, and exceptional activity. MoS_2 nanosheets have plenty of uses in gas barrier applications.

2.1. Synthesis methods of MoS_2 Nanosheets

2.1.1 Hydrothermal method

A Hydrothermal method is a typical method used for the synthesis of different nanomaterials like nanoparticles, nanorods, nanospheres, nanotubes, nanosheets, nanoflowers, etc. It is based on solution-rection phenomena. Materials with high- and low-pressure conditions can easily synthesize without affecting their structure by this method. The same is the case with temperature. The hydrothermal approach deals with a wide range of temperatures during synthesis. Nanomaterials that are unstable at their elevated temperature can be synthesized by this method and it is one of the advantages of the hydrothermal method. In this approach, salts of transition metals are mixed by a molar ratio of 1:2. The mixture is stirred with organic solvent and then transfer to the autoclave for heating., Conditions like temperature, time, etc. depend on the type of nanomaterial being used for synthesis. For the further process of nanomaterials, washing, drying centrifugation, sonication, etc. are used depending upon the type of nanomaterial. Let's take a look at different publications regarding MoS_2 nanosheet synthesis.

The paper by H. Liu et al reported the synthesis of MoS_2 nanosheets by the hydrothermal method. 0.076g of Ammonium molybdate tetrahydrate and 1.0g of thiourea were mixed with 30ml Deionized water (DI water). The carbon fiber piece was also mixed with the mixture. The solution was then transferred to an autoclave having 200° C temperature for 12 hrs. The mixture is then dried overnight at 60° C and after that calcination takes place at 400° C for 2hrs. With strong and sharp diffraction peaks, the calcination treatment enhances the phase crystallinity of MoS_2. The challenge in this paper was to boost zinc-ion interaction in nanosheets. In Kumar, Singh, Sharma, and Varma's publication MoS_2 nanosheets were synthesized for energy storage of practical supercapacitors by mixing 1g of H2NCSNH2, 1.1g of Na2MoO4.2H2O, and 12M HCL with 35ml DI water. The mixture was then stirred for 20 mins. The resultant solution was then led to an autoclave having 200°C for 24 hrs. Finally, drying occurs at 80° C for 12 hrs.

In Kasinatha n et al work the synthesis was carried out by adding 0.23g of Na2MoO4.2H2O and 0.8g L-cysteine in 50ml DI water and stirring at 25° C for 40 mins. Then the mixture was transferred to an autoclave at 180° for 24 hrs. After that, the sample was dried at 60° C for 12 hrs. In this paper calcination also takes place at 400° C for 4hrs. This method confirmed that MoS_2 has a multilayered 2D structure. Here Mos_2 nanosheets were used for biomedical applications. In this paper, Abinaya et al reported the synthesis of Mos_2 nanosheets by stirring the mixture of 4.5g of CSN2H4, and 2.5g of (NH4)6MoO7.4H2O NaOH, and 72 ml DI water for 30mins. The solution was then transferred to stainless steel chamber where the reaction occurs at 180° C for 24hrs. In the end, drying was done in 24hrs at 60° C. The creation of the 2H hexagonal phase has been established. The objective of this paper is to enhance the thermoelectric performance of Transition Metal dichalcogenides (TMDs).

Xu et al publish their research on the fabrication of triethylamine sensors using MoS_2/ZnO. Here MoS_2 was synthesized by mixing CH4N2S, Na2MoO4·2H2O by molar ratio 3:1 and 1mM CTAB with 10mM Citric Acid in 25ml DI water. Firstly, it was stirred for 3h and then an autoclave reaction occurred at 180° C for 22hrs. After the reaction, the desired nanosheets were then annealed under Nitrogen gas (N2) at 600° for 2hrs. The prepared samples' purity and crystal phase were determined. In the research publication of M.-C.

Liu et al, 121g of Na2MoO.2H2O and 1.52g of CH4NS were mixed with 60ml DI water to synthesize nanosheets for enhancing the performance of sodium ion storage. The process was started in an autoclave at 200° C for 24hrs. Then DI water and ethanol were used to wash the solution before drying at 50° C overnight. Vertical growth of MoS_2 nanosheets in a 2D accordion-structure was confirmed.

Jlidi, Baachaoui, Raouafi, and Ridene used 1.24g of Ammonium heptamolybdate and 2.28g of thiocarbamide as a precursor, and 36ml DI water as solvent. This mixture was then gone for reaction in an autoclave at 150°, 280°, or 200° C for 24hrs. The next solution was cooled for 2hrs at room temperature. Then DI water and ethanol were used to wash the solution before drying at 60° C vacuum drying. Using this method, the nanosheets were 2D crystalline in structure The challenge was to study the effect of temperature on different MoS¬2. In the paper Rahman, Samanta, Pathak, and Nath reported the synthesis of MoS_2 by mixing 2mM of Na2MoO4·2H2O and 5mM of CH4N2S with 40ml DI water. The solution was stirred for 30mins and then moved to an autoclave for reaction at 200° C for 24hrs which was then cooled naturally. After that, it was centrifuged for 30 mins and then washed with ethanol and water. In the end, the resultant solution was dried at 80° C overnight. To verify the production of crystalline phases of MoS_2 nanosheets, the room temperature patterns of undoped and Co-doped MoS_2 nanostructures of various doping concentrations were observed. The purpose of the paper was to modify optical and structural features in Co-doped Mos¬¬2 nanosheets.

Xiao et al published their work for efficient Electrocatalytic Hydrogen Evolution. The Synthesis approach was done by adding 0.2471g of (NH4)6Mo7O24.4H2O and 0.1461g of adipic Acid and 3ml Graphene Oxide which act as filler with 60 ml DI water and the solution was magnetically stirred for 10 mins. After that 0.853 g of Thiourea was added and stirred again for 10mins which was then moved into a Teflon-lined autoclave having 200° C temperature for 30hrs. The resultant is then cooled naturally and washed 3 times with DI water and ethanol. Lastly, vacuum drying occurred for 23hrs at 60° C. The structure of MoS_2 nanosheets was found to be hexagonal. The publication by Yu, Wang, Ni, Li, and Technology reported the synthesis of 1T-2HMos¬2 nanosheets by mixing 0.42mmol of (NH)4MoO4.4H2O and 6.4mmol of CS(NH2)2 with 15ml DI water. The

sample was moved to an autoclave for 24hrs at 180° C. Before doing vacuum drying at 120° C, it was washed with DI water or ethanol. The 2H-MoS_2 was further annealed at 700° C. 1T—2H MoS_2 nanosheets have a poor crystallinity. After thermal annealing at 700°C, the crystallinity of 2H—MoS_2 nanosheets improves dramatically. The objective of this work was to get better sodium storage.

P. Zhou et al in his work described MoS_2 nanosheet's synthesis by adding Na2MoO4.2H2O) and C2H5NS in 50ml DI water which was then stirred for 10mins. The sample was then transported to an autoclave at 180° C for 24hr which is then centrifuged. After that washing was performed with ethanol/DI water and then dried by using an electric oven in an Ar environment at 60° C for 12hrs. A layered structure with several parallel nanoflakes with a width of 0.7–1 m and a thickness of around 50 nm, was observed. The challenge in the work was to enhance visible light retort for Xanthates. In the paper by M.-C. Liu et al, 1.2097g of Na2MoO.2H2O and 1.5224g CH4NS were dissolved in 60ml DI water to synthesize MoS_2 nanosheets for the effective performance of sodium ion storage. The sample was moved to an autoclave where the reaction temperature was 200° C for 24hrs. washing was performed with DI water and Ethanol which was then dried at 50° C overnight. Vertical growth of MoS_2 nanosheets in a 2D accordion-structure Ta4C3 mechanical matrix resulted in a 3D M-Ta4C3 heterostructure.

Luo, Li, Guo, and Wu reported synthesis by mixing 0.5g of Na2MoO4.2H2O and 1g of CH4N2S in 30ml DI water. The sample was reacted in an autoclave at 230° C for 24hrs which was then cooled at room temperature. After that, it was passed through vacuum filtration and washed with ethanol or DI water. Drying was performed at 60° C for 12hrs and then annealed for 2hrs at 3° C-850° C. Results suggested that MoS_2 nanosheets were significantly thinner and smaller. The objective was to use nanosheets for the high-capacity anode. The paper by Liu, Pan, Deng, Xiang, and Lu reported synthesis by adding 30ml DI water in the mixture of 0.25g(NH4)6Mo7O24.4H2O and 1g of CS(NH2)2. The solution is then transferred to an autoclave for 24hrs at 200 C. After that Cooling was done at room temperature and washed with ethanol and DI water. The sample was then dried at 60° C for 12hrs. The purpose was to use nanosheets for highly effective microwave absorption.

2.1.2 Liquid Phase Exfoliation Method

Huang et al proposed the synthesis of MoS_2 nanosheets using the LPE method by adding 200 mg MoS_2 bulk with 200 mL NMP. The sample was sonicated for 7 h and then the solution was let for settling for 12 h. After that, it was centrifuged at 1500 and 10000 rpm for 45 and 10 min respectively. The collected amount was washed with distilled water. And the MoS_2 nanosheets were freeze-dried for 48 h. The challenge in this research was to improve the performance of MoS_2 in photocatalytic hydrogen evaluation.

In the work by Y. Liu et al, nanosheets for the removal of Ps2+ in an aqueous solution were synthesized by mixing 5 mg/mL of MoS_2 in water. Sonication was performed for 20 h (250W) and then centrifuged at 3300 and 17930 rpm for 43 and 30 mins respectively. The sample was washed with DI water. Arefi-Oskoui et al reported synthesis by mixing 0.4 g MoS_2 40 mL NMP and tert-butanol (70/30 v/v). Probe sonication was done for 90 min with 3 s on and 1 s off. The solution was then centrifuged for 25 mins at 1500 rpm. The sample was freeze-dried. The challenge of the study was the evaluation of MoS_2 bulk and nanosheet catalysts for using battery bioassays.

In the study by M. Zhang et al MoS_2 nanosheets were synthesized by 50 mg MoS_2 in 50 mL NMP. The sample was sonicated for 4 h at room temperature and after that centrifugation and washing were performed. In the end, it was dried at 60 C overnight. The idea was to check the effectiveness of MoS_2 synthesis on visible-light-induced antibacterial effect.

R Zribi et al proposed synthesis by adding 0.15 mg/mL of MoS_2 and 0.045 mg/mL sodium cholate with water. The mixture was sonicated for 30 min by a probe sonicator and then decanted overnight. In the end, it was centrifuged at 1500 rpm for 15 mins. The purpose was to use nanosheets on electrodes for enzyme-free sensing.

In the study of Singh, Kumar, Verma, & Soni 50 mL NMP with 10 mg MoS_2 were used to synthesize MoS_2 nanosheets. First mixing and stirring were done. Then the sample was sonicated for 6,12 and 18 h. centrifugation occurred for 15 min at 8000 rpm. Propanol and water ere used to wash the sample and then dried at 70 C for 24h. The cost-effective use of MoS_2 nanosheets for sunlight photocatalytic activity was the challenge in this research.

Rayne Zribi et al synthesized nanosheets by adding 5 mg/mL bulk MoS_2 and 1.5 mg/mL sodium cholate in water. The mixture was sonicated for 30 mins using a horn sonication bath and then decantation was done overnight. The sample was centrifuged for 90 mins at 1500 rpm. MoS_2 nanosheets were used in carbon electrodes

In this study R, Zribi et al used 0.15 mg/mL MoS_2 and 0.045 mg/mL sodium cholate with water to synthesize it. The sample was sonicated for 30 mins. Decantation was done overnight. The sample was centrifuged at 1500 rpm for 15 mins. Carbon and gold printed electrodes were modified by MoS2 nanosheets. Kaushik, Tiwari, Choubey, Singh, & Sinha proposed a study of MoS_2 synthesis using the LPE method. 30 mg MoS_2 and 10 mL NMP were taken and sonicated for 5h. the sample was then centrifuged for 20 mins at 8000 rpm. Karmakar, Sarkar, Tiwary, Kumbhakar, & Compounds published their work on MoS_2 nanosheets in triboelectric energy catalytic harvesting. They synthesized nanosheets by adding 150 mL DI water and bulk MoS_2 followed by 30 mins stirring. The resultant solution was again stirred with 0.75 g MoS_2, 25 mg of detergent powder, 200 microliters bellyache bush juice extract, and 200 microliter washout extract for 15 mins. 17W sonicator was used for 2 h to sonicate the sample and it was then centrifuged at 10000 rpm for 10 mins. The sample was washed with ethanol, acetone, and DI water to remove un-exfoliated MoS_2. To get the required nanosheets sample for dried at 80 C for 12 h. antibacterial activity through MoS_2 nanosheets was studied by Roy et al. 18 mL DI water and 12 mL chitson with 60 mg bulk MoS_2 and 5 mg/mL chitson were used to synthesized nanosheets. The sample was first sonicated for 20 mins in a bath sonicator and then probe sonication was performed for 4 h with 15 min on and off to break the layered structure of bulk MoS_2. in the end solution was centrifuged at 10000 rpm for 30 mins to get the required sheets.

Yao et al proposed their research work for MoS_2 nanosheets to improve ZnO rods' photocatalytic activity. The synthesis process was done by taking 800 mg MoS_2, 0.4 mL NMP and 20 mL ethanol-water mixture with 45 vol percent. MoS2 with 0.4 mL NMP was first grounded for 0.5,1,2 and 3 h which was the dried at 60 C in a vacuum oven. To break the layered structure sonication was performed for 3,10,20,60 and 120 mins. The desired product was achieved with centrifugation at 6000 rpm for 30 mins.

In the research by Ma, Zhang, Wu, Zhang, & Zeng nanosheets were synthesized for electrochemical sensing. The process starts by sonicating 2 mg/mL bulk MoS_2 in DMF for 6 h with 3 s on and 2 s off amplitude. The solution was then centrifuged at 1500 rpm for 45 rpm and 12000 rpm for 30 min. to get the desired nanosheets sample dried for 24 h at 50 C.

Wu, Liu, & Cheng published their work to improve the friction properties oi oil through MoS_2 nanosheets. LPE synthesis was carried out by mixing 0.73 g of bulk MoS_2, 1.22 g of LiOH, and 1.02 g of NaOH in 180 mL of water. The resultant mixture was first stirred for 2 h at room temperature and then 3 h at 100 C in three-necked flasks. A bath sonicator was used for 2 h to break the layered structure. The sample was let for settling for 2 h. nanosheets were collected after drying at 60 C for 24 h.

Santalucia et al published their work on a comparison of MoS_2 nanosheet synthesis. Three different solutions were made by taking water and ethanol (10 mL, 5.5 mL, and 4.5 mL) with 2 mg bulk MoS_2 powder. At the first bath, sonication was performed for 5 minutes, and then it was probe sonicated for 6 h with 30% amplitude. Desired nanosheets were collected after centrifugation at 4000 rpm for 30 mins.

2.1.3 Chemical Lithium Intercalation Method

H. Li et al reported chemical lithium intercalation method used MoS_2 catalyst for ammonia synthesis. The sample was prepared by dissolving 1 g MoS_2 in 60 ml n-butyl lithium/ n-hexane and stirred for 1 h. Hexane was used to remove excess material. To exfoliate nanosheets 1 h sonication was performed, and, in the end, it was centrifuged.

In the work by W. Xu et al MoS_2 synthesis was carried out by taking 0.4 g MoS_2 in 2 mL n-BuLi /hexane. The solution was sonicated for 3 h in Ar atmosphere and sonicated in Ar saturated water. The final nanosheets were obtained from centrifugation of 12000, 5000, and 12000 for 40, 30, and 60 min. the purpose of the study was to use nanosheets in hydrogels.

2.1.4 Solid State Method

Chen et al reported their work to improve visible-light photoactivity through MoS_2 ultrathin nanosheets. The solid-state method was used to synthesize MoS_2 nanosheets. The

solution was prepared by adding 20 mL water to the mixture of 1 g SiO2 0.3 g (NH4)6MoO24.4H2O and 0.3 g S powder which was dried at 60C and stirred. Vulcanization was carried out in a tubular furnace at 400 C for 2 h (20 C/min). the solution was immersed in 30 mL of 10% Hf aqueous solution for 6 h. then the sample was washed with water, CS2, ethanol, and distilled water to remove impurities, and finally, it was dried at 60C

2.1.5 Solvent Thermal Method

Chen et al mentioned the solvent thermal method of hybrid MoS_2 nanosheets for photocatalytic H2 production. Synthesis was carried out by mixing 100 g g-C2N4/(NH4)2MoS4 with DMF and transferred to an autoclave for 24 h at 210 C solution was then cooled at room temperature and centrifuged at 10000 rpm for 10 min. vacuum drying was carried out at 60 C and the resultant product was washed with ethanol 3 times.

synthesis of MoS_2 nanosheets was reported by Alomar, Liu, Chen, & Fida for photocatalytic activities. The sample was prepared by mixing 0.99 g (NH4)6Mo7O24.4H20 and 0.5 g of (NH2)2CS in 20 mL ethylene glycol, 10 mL ethanol, and 15 mL water. Which was then stirred for 10 mins up to 40%. An autoclave was used for the reaction of the solution at 200 C for 6 h. the solution was then cooled and washed with water-ethanol to get the desired product. It was dried at 80 C for 24 h

2.1.5 Electrochemical Exfoliation Method

W. Wu et al reported their work for high-performance lithium storage using MoS_2 nanosheets by electrochemical exfoliation. They proposed a synthesis process by mixing MoS_2 and 1M sodium sulfate with water. The mixture was first sonicated for 60 min. and then filtered with titanium (100 mesh) and propylene (12500 mesh, bore diameter 0.1 micrometers) after that mixture was immersed in 1M sodium sulfate aqueous solution. Electrochemical exfoliation was carried out at 20W (room temperature) to break the layer structure the resultant solution was probe sonicated for 2 h and then again filtered under vacuum. Ethanol and DI water were used to wash that mixture and then centrifugation occurred at 3000 rpm for 10 mins. In the end, the solution was freeze-dried.

Table 1: Synthesis Methods of MoS_2 Nanosheets

S.No	**Materials**	**Quantity of Material**	**Solvent**	**Methods**	**Conditions**	**Applications**	**REF**
1	Ammonium molybdate tetrahydrate: thiourea: Piece of carbon fiber	0.076g: 1.0g	DI water (30ml)	**Hydrothermal** • Drying • Calcination	**200°C/12h** • 60° overnight • 400°C/2h	Boosting zinc-ion interaction	[22]
2	H_2NCSNH_2: $Na_2MoO_4.2H_2O$: HCL	1.0g: 1.1g: 12M	DI water (35ml)	**Hydrothermal** • Stirring • Drying	**200°C/24h** • 20 mins • 80°C/12hr	Energy storage for practical supercapacitors	[23]
3	$Na_2MoO_4.2H_2O$: L-cysteine	0.23g: 0.8 g	DI water (50ml)	**Hydrothermal** • Stirring • Drying • Calcination	**180°C/24h** • 25°C/40 mins • 60°C/12h • 400°C/4h	Biomedical (MCF-7 breast cancer & pathogenic bacteria)	[24]
4	CSN_2H_4: $(NH_4)_6MoO_7.4H_2O$: NaOH	4.5g: 2.5g	DI water (72ml)	**Hydrothermal** • Stirring • Drying	**180°C/24h** • 30 mins • 60°C/24h	Enhancing the thermoelectric performance of TMD	[25]
5	CH_4N_2S: $Na_2MoO_4{\cdot}2H_2O$: CTAB: Citric Acid	3M: 1M: 1mM: 10mM	DI water (25ml)	**Hydrothermal** • Stirring • Annealing under N_2	**180°C/22h** • 3h • 600°C/2h	Fabrication of triethylamine (TEA) sensor using MoS_2/ZnO	[26]
6	$Na_2MoO.2H_2O$: CH_4NS	1.21g: 1.52g	DI water (60ml)	**Hydrothermal** • washing • Drying	**200°C/24h** • DI water/Ethanol	Enhancing the performance of sodium-ion storage	[27]

					• 50°C/over night		
7	Ammonium heptamolybdate: thiocarbamide	1.24g: 2.28g	DI water (36ml)	**Hydrothermal** • Cooling • Washing • Drying	**150, 280 0r 200°C/24h** • 25°C/2h • DI water/Ethanol • 60°C vacuum drying	Effect of temperature on optical, structural, and morphological properties of MoS_2	[28]
8	$Na_2MoO_4 \cdot 2H_2O$: CH_4N_2S	2mM: 5mM	DI water (40ml)	**Hydrothermal** • Stirring • Cooling • Centrifugation • Washing • Drying	**200°C/24h** • 30 mins • Naturally • 30 mins • Ethanol/water • 80° C overnight	Modification in optical and structural properties in Co-doped MoS_2 Nanosheets	[29]
9	$(NH_4)_6Mo_7O_{24}.4H_2O$ CH_4N_2S	0.35g 0.76g	DI Water 15ml	**Hydrothermal** • Sonication • Centrifugation • Washing • Drying	**200°C/8h** • 30 mins • Time not mentioned • Ethanol/ Water • 60° C 12 hrs.	Remediation of Pd (II) & Hg (II) by MoS_2	
10	$(NH_4)_6Mo_7O_{24}.4H_2O$ Adipic Acid	0.2471g 0.1461 g	DI Water 60ml	**Hydrothermal** • Stirring • Cooling • Washing	**200°C/30h** • 10 mins • Naturally	MoS_2 for Efficient Electrocatalytic	[30]

				• Drying	• Ethanol/DI Water • 60° C Vacuum drying 23 hrs.	Hydrogen Evolution	
11	$(NH)_4MoO_4.4H_2O$ $CS(NH_2)_2$	0.42 mmol 6.4 mmol	DI Water 15 ml	**Hydrothermal** • Washing • Drying	**180°C/24h** • Ethanol/DI Water • 120° C Vacuum drying	MoS_2 hybrid Electrodes for better sodium storage	[31]
12	$Na_2MoO_4.2H_2O$) C_2H_5NS	-	DI Water 50 ml	**Hydrothermal** • Stirring • Centrifugation • Washing • Calcination • Drying	**180°C/24h** • 10 mins • - • Ethanol/DI Water • AR environment • 60° C Electric oven 12h	MoS_2 for enhancing Visible Light Response for Xanthates	[32]
12	$Na_2MoO.2H_2O$ CH_4NS	1.2097 g 1.5224 g	DI Water 60 ml	**Hydrothermal** • Washing • Drying	**200°C/24h** • Ethanol/DI Water • 50° C overnight	MoS_2 for efficient performance sodium ions storage	[27]
13	$Na_2MoO_4.2H_2O$) CH_4N_2S	0.5 g 1 g	DI Water 30 ml	**Hydrothermal** • Cooling • Filtration	**230°C/24h** • Room temperature	MoS_2 nanospheres for high-capacity anode	[33]

				• Washing • Drying • Annealing	• Vacuum • Ethanol/DI Water • 60° C 12h • 3°C-850°C 2h		
14	$(NH_4)_6Mo_7O_{24}.4H2O$ $CS(NH_2)_2$	0.25 g 1 g	DI Water 30 ml	**Hydrothermal** • Cooling • Washing • Drying	**200°C/24h** • Room temperature • Ethanol/DI Water • 60° C 12h	MoS_2 for high-efficiency microwave absorption	[34]
15	$Na_2MoO_{24}.2H_2O$, 99% NH_2CSNH_2	1 g 1.4 g	DI Water 80 ml	**Hydrothermal** • Stirring • Cooling • Washing • Drying	**200°C/24h** • - • Room temperature • Ethanol/DI Water • 80° C	MoS_2 used as a Nao catalyst for synthetic dye degradation	[35]
35	MoS_2	200 mg	NMP 200 ml	**Liquid Phase Exfoliation** • Sonication • Settling • Centrifugation • Washing • Drying	• 7 h • 12 h • 1500 & 10000 rpm 45 & 10 mins • Distilled Water	Performance of MoS_2 in photocatalytic hydrogen evolution.	[36]

					• 48 h Freeze-drying		
36	Mos_2/ Sodium Cholate	5 mg/mL 1.5 mg/mL	Water -	**Liquid Phase Exfoliation** • Sonication • Centrifugation • Washing Drying	• 20 h (250W) • 3300 & 17930 rpm 43 & 30 mins • DI Water	MoS_2 nanosheets for removal of Pb^{2+} in aqueous solution	[37]
37	MoS_2	0.4 g	NMP/ Tert-butanol 40 mL 70/30 v/v	**Liquid Phase Exfoliation** • Sonication • Centrifugation • Drying	• 90 min (200W) (3 s on & 1 s off) • 1500 rpm 25 mins • Freeze-dried	Evaluation of MoS_2 bulk and Nanosheets catalysts using battery bioassays	[38]
38	MoS_2	50 mg	NMP 50 mL	**Liquid Phase Exfoliation** • Sonication • Centrifugation • Washing • Drying	• 4 h (Room temperature) • - • - • 60 °C overnight	Effect of MoS_2 synthesis on visible-light-induced antibacterial effect.	[39]
38	MoS_2 Sodium cholate	0.15 mg/mL 0.045mg/mL	Water	**Liquid Phase Exfoliation** • Sonication	• 30 mins	MoS_2 nanosheets on electrodes for enzyme-free sensing	[40]

				• Decantation • Centrifugation	• Overnight • 1500 rpm 15 mins		
39	MoS_2	10 mg	NMP 50 ml	**Liquid Phase Exfoliation** • Stirring • Sonication • Centrifugation • Washing • Drying	• - • 6, 12, 18 h • 8000 rpm 15 mins • Water/ Propanol • 70 °C 24 h	Cost-effective use of MoS_2 nanosheets for sunlight photocatalytic activity	[41]
40	$M0S_2$/ Sodium cholate	5 mg/mL 1.5 mg/mL	Water	**Liquid Phase Exfoliation** • Sonication • Decantation • Centrifugation	• 30 mins • Overnight • 1500 rpm 90 mins	MoS_2 nanosheets used in carbon electrodes	[42]
41	$M0S_2$ Sodium cholate	0.15 mg/mL 0.045 mg/mL	Water	**Liquid Phase Exfoliation** • Sonication • Decantation • Centrifugation	• 30 mins • Overnight • 1500 rpm 15 mins	MoS_2 nanosheets used in carbon & gold printed electrodes	[40]
42	$M0S_2$	30 mg	NMP 10 ml	**Liquid Phase Exfoliation** • Sonication	• 5 h	Study of MoS_2 synthesis	[43]

				• Centrifugation	• 8000 20 mins		
43	$M0S_2$ Detergent powder Bellyache bush juice extract Washout extract	0.75 g 25 mg 200 µl 200 µl	DI Water 150 ml	**Liquid Phase Exfoliation** • Stirring • Stirring • Sonication • Centrifugation • Washing • Drying	• 30 min • 15 min • 2 h (17W) • 10000 10 mins • Ethanol Acetone & DI Water • 80 °C 12 h	MoS_2 nanosheets in triboelectric catalytic energy harvesting	[44]
44	MoS_2/ Chitson	60 mg 5 mg/mL	DI Water 18 mL Chitson aqueous solution 12 mL	**Liquid Phase Exfoliation** • Sonication (Bath) • Sonication (probe) • Centrifugation	• 20 min • 4 h 15 min on/off • 5000 45 min/ 10000 30 min	Antibacterial Activity through MoS_2 nanosheets	[45]
45	MoS_2	800 mg	45% Ethanol/water mixture 20 mL	**Liquid Phase Exfoliation** • Grinding • Drying • Sonication	• 0.5, 1, 2 & 3h • 60 °C Vacuum Oven • 3, 10, 20, 30, 60, & 120 min	Enhancing ZnO rod's photocatalytic activity by MoS_2 nanosheets	[46] [47]

				• Centrifugation	• 6000 rpm 30 min		
46	MoS_2	2 mg/mL	DMF	**Liquid Phase Exfoliation** • Sonication • Centrifugation • Drying	• 6 h (130W0 3s on & 2 s off) • 1500 rpm 45 min 12000 rpm 30 min • 50 °C 24h	MoS= nanosheets for electrochemical sensing	[48]
47	MoS_2 LiOH NaOH	0.73 g 1.22 g 1.02 g	DI Water 180 mL	**Liquid Phase Exfoliation** • Stirring • Stirring • Sonication (bath) • Settling • Drying	• 2 h Room temperature • 3 h 100 °C (three-necked flask) • 2 h • 30 min • 60 °C 24 h	Enhancing friction properties of oil through MoS_2 nanosheets	[49]
48	MoS_2	2 mg	Water/Ethanol 10 mL (5.5 mL & 4.5 mL)	**Liquid Phase Exfoliation** • Sonication (bath)	• 5 min (20 kHz)	Comparison of MoS_2 nanosheets synthesis	[50]

				• Sonication (probe) • Centrifugation	• 6 h (500W) 30% amplitude • 4000 rpm 30 min		
49	MoS_2	1 g	n-butyl lithium/n-hexane 60 mL (2.4M n-butyllithium hexane	**Chemical Lithium Intercalation Method** • Stirring • Washing • Sonication • Centrifugation	• 1 h • Hexane • 1 h • -	MoS_2 as a catalyst for ammonia synthesis	[51]
50	MoS_2	0.4 g	n-BuLi hexane (2.4) 2 mL	**Chemical Lithium Intercalation Method** • Sonication • Sonication • Centrifugation	• 3 h (Ar atmosphere) • Ar-saturated water • 12000, 5000, 12000 rpm 40, 30,60 min	MoS_2 nanosheets in hydrogels	[52]
51	SiO_2 $(NH_4)_6MoO_{24}.4H_2O$	1 g 0.3 g	Water 20 ml	**Solid-State Method** • Drying & stirring	• 60 °C – • 400 °C (20 C/min) 2h	Improving visible light photoactivity through MoS_2	[53]

	S powder	0.3 g		• Valcunize (Tubular furnace) • Immersing • Washing • Drying	• 6 h (30 mL of 10% HF aqueous solution) • Water/CS 2/ethanol/ distilled water • 60 °C	ultrathin nanosheets	
52	g-C_3N_4/ $(NH4)_2MoS_4$	100g -	DMF	**Solvent Thermal Method** • Cooling • Centrifugation • Drying • Washing	**210°C/24h** • Room temperature • 10000 rpm 10 mins • 60 °C Vacuum oven • Ethanol	Hybrid MoS_2 nanosheets for photocatalytic H_2 Production	[54]
53	$(NH_4)_6Mo_7O_{24}.4H2O$ $(NH_2)_2CS$	0.9 9 0.5 g	Ethylene glycol 20 m l Ethanol 10 mL Water 15 mL d	**Solvent Thermal Method** • Stirring • Cooling • Filtration	**200°C/6h** • 40 % 10 mins • Room temperature • -	MoS_2 Nanosheets for photocatalytic activities.	[55]

				• Washing • Drying	• Water & ethanol • 80 °C 24 h		
54	MoS_2 Sodium sulfate	- 1M	Water -	**Electrochemical Exfoliation** • Sonication • Filtration • Immersing • Electrochemical Exfoliation • Sonication (tip) • Filtration • Washing • Centrifugation • Drying	• 60 mins • Titanium (100 mesh) & Polypropylene Membrane (125000 mesh, pore diameter ca. 0.1 µm) • 1M Sodium sulfate aqueous solution • 20.0 V Room temperature • 2h • Vacuum • DI Water & ethanol • 3000 rpm 10 mins • Freeze drying	MoS_2 nanosheets for high-performance lithium storage	[56]

PET/organo clay nanocomposite was synthesized, and the clay was modified with methyl tallow bis(2-hydroxyethyl) ammonium having a commercial name of Nanofin(DK2). PET with an intrinsic viscosity of 0.81 dL/g was used. Nanocomposites were prepared using melt compounding technique in a twin-screw compounder with various wt.% of clay, 68.8% reduction in O_2 permeation for 5wt.% composite was reported, whereas 1wt.% showed 22.6% reduction and 3wt.% showed 14.2% respectively. They concluded that a higher reduction in permeability of 1wt.% organoclay as compared to 3wt.% was due to the higher and better exfoliation at lower clay percentages [57].PET nanocomposites were prepared using two organoclays namely Cloisite 15A and Nanolin DK2 via melt blending technique and were tested for their permeability with different weight percentages, among all compositions, 1wt.% of Nanolin/PET composite showed the highest reduction in permeability with 44.8%, whereas 2wt.% Cloisite/PET composite showed the superior barrier properties of all Cloisite/PET composites with a 29.59% decrease in O_2 permeation as compared to the bottle-grade PET. Furthermore, in their final remarks, they inferred that the higher the degree of exfoliation, the lower the permeability and the lower the wt. % of clay, higher is the exfoliation [58].

PET/Na^+MMT composites were synthesized using esterification clay addition (ES clay addition) and polycondensation (PC) clay addition (PC clay addition), better results in permeation with lower percentage composites of PET/Na^+MMT in the ES clay addition method were observed as a contrast to PC method due to better exfoliation and dispersion of clay in former, and a highest of 36 % reduction in oxygen permeability with 0.5wt.% PET/Na^+MMT composite was achieved [59].PET/PEN composites were prepared with 50/50 composition using ultrasonically aided extrusion and Oxygen permeation at different ultrasonic amplitudes varying from (0-10) µm was noted. 40% reduction in O_2 permeability coefficient at 0 µm amplitude was observed and it was concluded that ultrasonication did not affect the 50/50 PET/PEN composite [60].PET/MXD6/Clay(D72T) composites were synthesized using 4 methods and their barrier properties were observed: a blend of PET/MXD6 having a weight ratio of 9:1 was used as a polymer matrix. PET/MXD6 blend was found to have a 25.4% lower O_2 permeability constant than pure PET owing to the superior gas barrier properties of MXD6, the addition of 3.5wt.% clay resulted in the

further reduction of permeability constant by 10-20%. An overall 40-45% reduction in permeability constant was achieved using different wt.% of PET/MXD6/Clay composite. It was concluded that when PET-clay is extruded first and followed by MXD6 addition, the clay is more homogeneously distributed and intercalated among two polymer phases (PET & MXD6) and the permeability constant is at its lowest [61].

PET/MMT composites were formed using the melt blending technique with 5wt.% MMT and a comparative study of PET nanocomposite versus nanocomposites of biopolymers were performed. OTR test at 0%RH (Relative Humidity) for the 5wt.% PET/MMT yielded a 55% reduction in O_2 permeability, and a 35% reduction at 80% RH for the same nanocomposite compared to pure PET, it was also reported that a Nano-bio composite blend of PHB/PCL had exhibited better oxygen, water, and limonene barrier properties than pure PET. However, 5wt.%PET nanocomposite was observed to have the lowest permeability of all the nanocomposites[62]. PET/Na-MMT nanocomposite with different compositions was prepared using the melt blending technique and it was found that oxygen permeation reduction increased until 2wt.% with the highest reduction of 52% and decreased when the wt.% was further increased, 5wt.% showed only a 37% decrease, which could have been due to the presence of tactoid structures as suggested by the authors. In 0.5, 1, and 2 wt.% composites the clay was better exfoliated, whereas, in 3 and 5 wt.% composites, clay was partially exfoliated and partially intercalated, which might have been the reason for their inferior O_2 barrier properties [63].

Recent years have seen a growing interest in using graphite derivatives due to their extremely high aspect ratios, in contrast to organoclays, graphene nanosheets have 25-130 times high gas barrier properties [64]. PET/FGO and PET/GO nanocomposites were synthesized using solution blending. GO was prepared using the Hummers process and it was functionalized via nucleophilic substitution using alkyl bromide to convert the hydrophilic groups such as hydroxyl, epoxy, and carboxylic acid to alkyl and alkyl ether. A 38% reduction in permeation of O_2 with 1wt.% PET/GO composite and 97% reduction with 3wt.% PET/FGO composite as compared to pure PET was achieved, greater reduction in FGO composites was reported to be due to homogeneous dispersion of graphene in PET [65]. PET/GNP(Graphite Nanoplatelets) nanocomposites of different compositions were

prepared using melt compounding, and it was reported that the composites prepared via quenching had a lower degree of crystallinity and it was also observed that the oxygen permeability is reduced by the presence of GNP and by the degree of crystallinity. 99% reduction in O_2 permeation using 1.5wt% was also claimed, the highest so far [66].PET/Cloisite 30B nanocomposites were prepared with varying wt.%, using in-situ polymerization and a highest of 50% reduction in O_2 permeation with 3wt.% composite was achieved [67]. PET/GO nanocomposites at low loadings (0.1-0.5wt%) were prepared by in-situ polymerization and it was noted that the PET nanocomposites had oxygen barrier properties superior by a factor of 2-3.3 as compared to pristine PET, a highest of 69.6% reduction in O_2 permeation with 0.5wt.% nanocomposite was reported [68].

Table 2: Effect of different nano fillers on gas barrier properties of PET polymer

Polymer	IV (dL/g)	Filler	Fraction	%Reduction in Permeability	Authors
PET	0.81	DK2	1wt.% 3 wt.% 5 wt.%	22.6(O_2) 14.2(O_2) 68.8(O_2)	[57]
PET	0.82	Cloisite 15A	1 wt.% 2 wt.% 3 wt.%	19.7(O_2) 29.59(O_2) 16.1(O_2)	[58]
PET	0.82	Nanolin DK2	1 wt.% 2 wt.% 3 wt.%	44.8(O_2) 29.59(O_2) 30.49(O_2)	[58]
PET	-	ES Clay addition	0.5 wt.% 2 wt.%	36(O_2) 29(O_2)	[59]
PET	-	PC Clay Addition	0.6 wt.% 2 wt.%	31(O_2) 25(O_2)	[59]
PET	0.74	PEN	50 wt.%	40(O_2)	[60]
PET	0.80	MXD6 Clay-MXD6	10 wt.% (3.5/10) wt.%	25.4(O_2) 41.31(O_2)	[61]

PET	-	MMT	5 wt.%	55(0% RH) (O_2) 35(80%RH) (O_2)	[62]
PET	0.84	Na-MMT	0.5 wt.% 1 wt.% 2 wt.% 3 wt.% 5 wt.%	28.7(O_2) 41.4(O_2) 51.7(O_2) 40.2(O_2) 36.8(O_2)	[63]
PET	0.80	GNP	0.1 wt.% 0.5 wt.% 1 wt.% 1.5 wt.%	-0.9(O_2) -18(O_2) 75.6(O_2) 99(O_2)	[66]
PET	-	GO	1 wt.%	38.19(O_2)	[65]
PET	-	FGO	1 wt.% 3 wt.%	85.18(O_2) 97.36(O_2)	[65]
PET	0.71	Cloisite 30B	2 wt.% 3 wt.% 5 wt.%	25(O_2) 50(O_2) 12.5(O_2)	[67]
PET	0.536	GO	0.1 wt.% 0.3 wt.% 0.5 wt.%	51.23(O_2) 61.72(O_2) 69.9(O_2)	[68]

Chapter 3 - Materials & Methods

N-methyl-2-Pyrrolidone (NMP), and Molybdenum disulfide were purchased from Sigma Aldrich. ECOPACK LTD supplied industrial-grade PET Poly(ethylene terephthalate) with an inherent viscosity of 0.81 dL/g.

3.2. Nanosheets Synthesis

In a cold water bath, 300mg of Molybedum disulfide powder was sonicated for 48 hours with 40mL of NMP in a metallic container using a 120hertz fixed frequency sonicator at 60amplitude with a 1sec on and 1sec off pulse. The resulting solution contained exfoliated nanosheets with varying aspect ratios, which were separated by centrifugation at 500rpm. The supernatant was collected in centrifuge tubes and vacuum filtered on a PTFE membrane with a 0.4-micron pore size to remove the excess NMP. The filtrate-containing membrane was then placed inside an oven at 60^{o}C overnight to obtain the desired nanosheets, and the same procedure was repeated at 1000rpm and 1500rpm. XRD and SEM were used to investigate nanosheets. The technique is also depicted in (Figure 5).

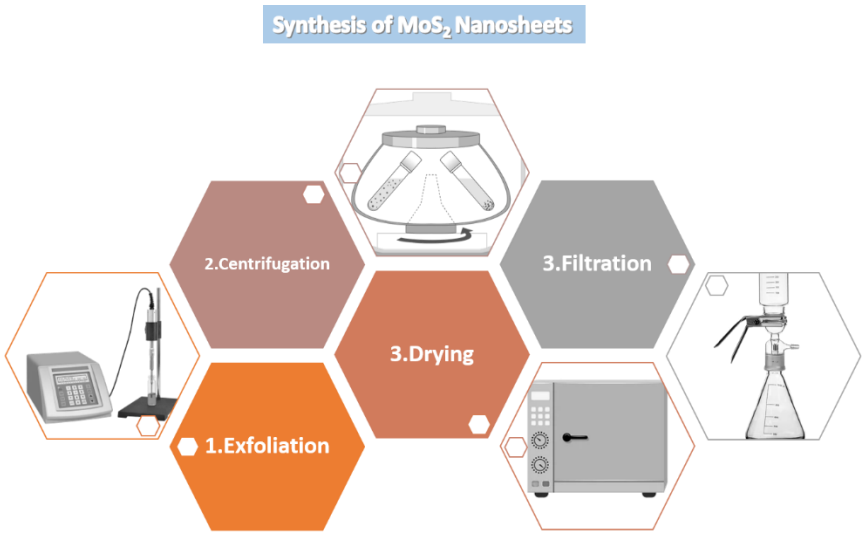

Figure 5: Molybdenum disulfide nanosheet synthesis

3.3. Nanocomposite film Synthesis

The composites were created on 500rpm, 1000rpm, and 1500rpm. MSNS. TIPS (Temperature-induced phase separation) was used to create PET membranes, pure and nanocomposites. PET pellets were dispersed in NMP at a temperature greater than its Tg (>165oC) with steady magnetic stirring (200rpm) within a 10ml glass vial. The solution concentration was fixed at 550mg/10mL. Pellets were seen to be completely dispersed after 35-40mins, nanosheets of the required concentration were then added, and the solution was magnetically stirred on the hot plate for another 15-20mins to ensure uniform dispersion of nanosheets inside the polymer matrix; however, the color of the solution was seen to change from transparent to dark yellow-brownish with time. This might be due to polymer chain disassociation and acetaldehyde production during heating [69]. Following that, the solution was carefully cast in a 4-inch glass petri dish and heated in an oven at a high temperature. As soon as the solvent evaporated, membranes with a thickness of 50-120um were created. PET nanocomposite samples ranging from 0.0025 to 0.02wt percent were created and analyzed for CO2 permeability. Membranes were found to be particularly sensitive to evaporation time and temperature, with a slight delay or early opening of the oven resulting in either a brittle or patterned membrane. (Figure 6) depicts the suggested procedure in further detail.

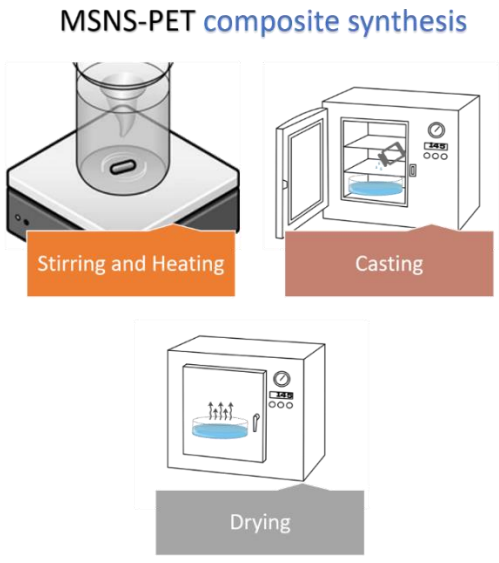

Figure 6: MSNS-PET nanocomposite synthesis

3.3.1. Optimization of Parameters for PET film synthesis

3.3.1.1. Temperature of Evaporation

Temperature adjustment for PET film synthesis may be classified into two categories: (1) above glass crystallization temperature (Tg) and (2) below Tg (Tg). Tg for amorphous PET is 67oC and 81oC for crystalline PET. Because the PET polymer employed in this study was semi-crystalline, as observed and demonstrated by XRD measurement, its Tg falls somewhere between 67 and 81oC. PET films created below Tg were entirely amorphous and brittle, making them unsuitable for testing; even the smallest touch with anything hard would cause them to break. PET films made above Tg in the 100-130oC range were rigid and stronger than films formed below Tg but were still inappropriate for permeation testing. Films made in the 130-150oC temperature range demonstrated increased strength. Furthermore, a temperature rise was linked to a decrease in pore size and distribution, as well as an increase in film density. For the permeation study, 145oC was chosen as the perfect and optimized temperature for PET film production, where strength, ductility, brittleness, and pore size were optimal. Furthermore, when the temperature rose, the look of the films changed from white (100-120)oC to brownish (120-200)oC. All PET nanocomposite films were made at an evaporation temperature of 145oC.

3.3.1.2. Duration of Evaporation

The evaporation time was optimized once the variable of evaporation temperature was established. The ideal period for 145oC was discovered to be roughly (1hr-1hr5)mins; if heated for even a minute longer, the film became too brittle to test and shattered at the slightest of interactions. It was also discovered that every 10oC increase in evaporation temperature resulted in a 10min decrease in evaporation time.

3.3.1.3. The amount of PET

PET films were created with PET concentrations ranging from 300mg/mL to 550mg/mL. PET films with concentrations ranging from 300mg/mL to 500mg/mL were found to be too thin to be tested for penetration. All PET nanocomposite films were then produced at a concentration of 550mg/10 mL, with thicknesses ranging from 50 to 110um.

3.3.1.4. Stirring speed and duration impact.

Preliminary PET film samples created had strange patches on the surface, which were supposed to be caused by MSNS non-uniform dispersion. To address the surface non-uniformity of the PET film, the stirring time and rpm for the dissolving stage were adjusted. The stirring duration was changed from 30mins to 1hr while maintaining the rpm constant at 500, and it was shown that the optimal stirring time for dissolution was 1hr since it greatly reduced non-uniformity. Any more stirring time would lead the PET, NMP, and MSNS combination to turn brownish, hurting the aesthetics. To improve the aesthetics of the PET film surface, rpm was adjusted while all other factors remained constant. The values varied from (100-500) rpm, and it was discovered that at higher rpm values, the dissolution time increased because PET pellets would rise in a glass vial and be farther from the heating plate surface, requiring more time to disperse, whereas at 100rpm PET pellets were on the bottom of the glass vial and thus near to the heating surface, requiring less time to dissolve. Because rpm affects stirring time, its indirect negative effect was reduced by maintaining the rpm value constant at 100. Even after optimizing these two variables, there was still some non-uniformity on the surface of the PET film.

3.3.1.5. Casting Position in the Oven

After seeing no substantial improvement in the aesthetics of the film's surface, it was considered that the problem remained due to non-uniform heating and, as a result, solvent evaporation. To address this issue, the location of the casting inside the ovens was optimized. PET films were cast in three separate ovens at 20 different places. It was discovered that position has a considerable influence on film aesthetics. All ovens had a distinct position where consistent heating and evaporation occurred, and these sites were not in the middle of the ovens. By optimizing this pattern, all of the areas caused by uneven heating were eliminated. Even after adjusting the casting sites, certain patterns remained on the surface of the films.

3.3.1.6. Effects of the glass vial's lid

This variable was the most difficult to predict having any effect on the surface look of the film of all the factors optimized. It was discovered that when films were cast with the dissolving stage conducted without the lid of the glass vial, all non-uniform patterns

vanished. The reason for this peculiar phenomenon is that when the solvent evaporates during the dissolving stage with the lid intact, it condenses on the inner surface of the lid owing to temperature differences. The condensed solvent then returns to the bulk mixture, thus at any point throughout the dissolving process, there was NMP in the bulk at a lower temperature than the remainder of the bulk temperature. When the lid was removed and the mixture was cast on a petri dish inside the oven, the colder NMP evaporated slower than the remainder of the NMP, resulting in patterns on the surface. The pattern problem was ultimately solved by removing the lid during the disintegration process.

3.4. Characterization

3.5.1. Tensile Testing Machine Operation

A material's tensile strength is the greatest stress that it can bear before breaking. Materials are classified according to their mechanical strength. Glassy and rubbery materials are examples of this. The classification of these two groups is based on their stress-strain response. Glassy materials are hard and brittle, but rubbery materials are pliable. The stress-strain response of different materials is seen in (Figure 7). The curve in this image indicates that brittle (glassy) materials have a high tensile strength, which is the end point of each curve shown, but only a minor amount of strain. The more flexible rubbery material, on the other hand, exhibits a high strain but a substantially lower tensile strength.

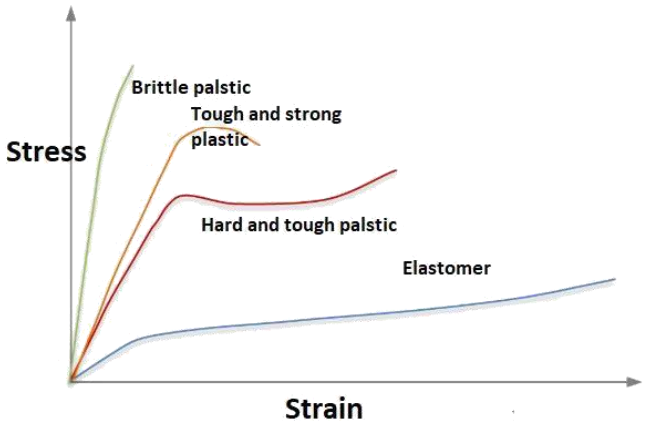

Figure 7: The stress-strain behavior of several classes of materials

The Tensile Testing Machine is used for determining the tensile strength of membrane materials. This machine is primarily composed of a load coupled to a moveable upper jaw, to which one end of our test material is secured. The fixed lower jaw is fastened to the base and is where the opposite end of the test material is secured. When the material is securely grasped by the two jaws, the computer attached to the machine sends the instruction to begin the test. The upward movement of the moveable upper jaw begins the progressive elongation of the material. The movement is regulated by the material's elongation rate, also known as the test speed because the elongation rate is proportional to the speed at which the upper jaw rises. The test is immediately terminated when the material breaks. The tensile testing machine's schematic diagram is illustrated in (Figure 8).

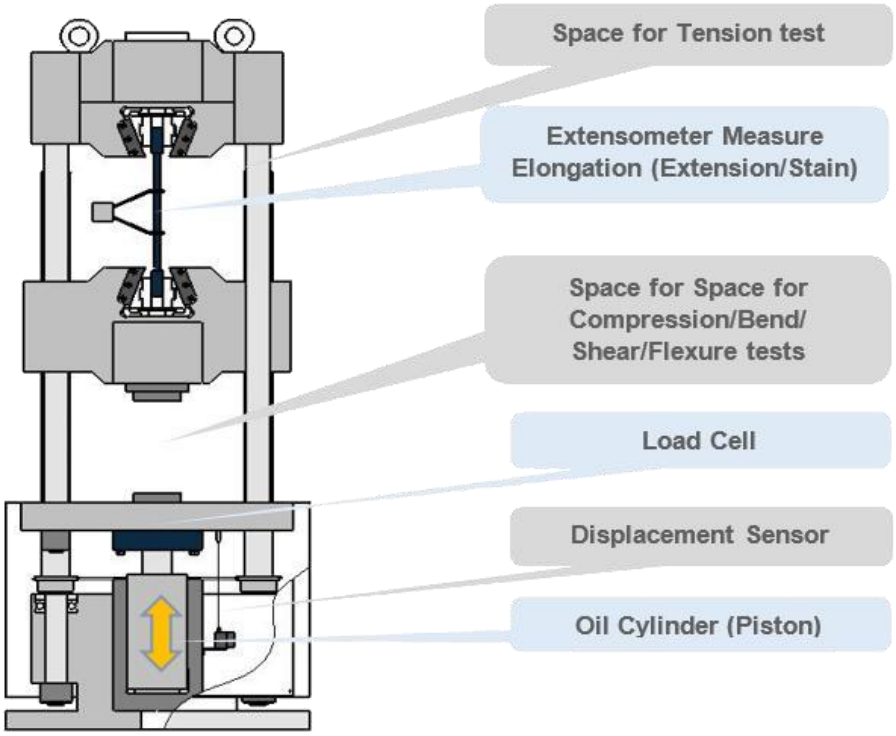

Figure 8: Schematic diagram of Tensile Testing Machine

Tensile testing was performed on all samples, 0.0025 percent, 0.005 percent, 0.01 percent, and 0.02 percent PET/MSNS films, using a SHIMADZU AGS-X series precision ultimate tensile tester with a full load of 20 kN. Because all of the samples were evaluated using the ASTM standard D882-02, the strips to be utilized were cut to the dimensions specified by

the standard. Finally, the stress-strain behavior of the tests performed using the aforementioned standard was investigated.

3.5.2. SEM Principles of Operation

The interaction of electrons with specimen material is the science underpinning scanning electron microscopy (SEM). When an electron beam is injected into a column of the Scanning Electron Microscope, it does not come into contact with any atoms of any gas or liquid in the environment since the column is vacuumed. Electrons do not interact with matter unless they come into contact with a dense solid substance. When an electron beam strikes a sample, part of its energy is transferred to the molecules in the sample. As a result, it is reflected at an angle relative to its initial well-defined course. As a result, backscattered electrons, secondary electrons, and X-rays are produced. These interactions provide critical information regarding the topography, composition, crystal structure, and existence of electrical and magnetic fields. All of these interactions result in electron scattering, which may be divided into two types: elastic and inelastic scattering, as seen in Figure 1. (Figure 3.5).

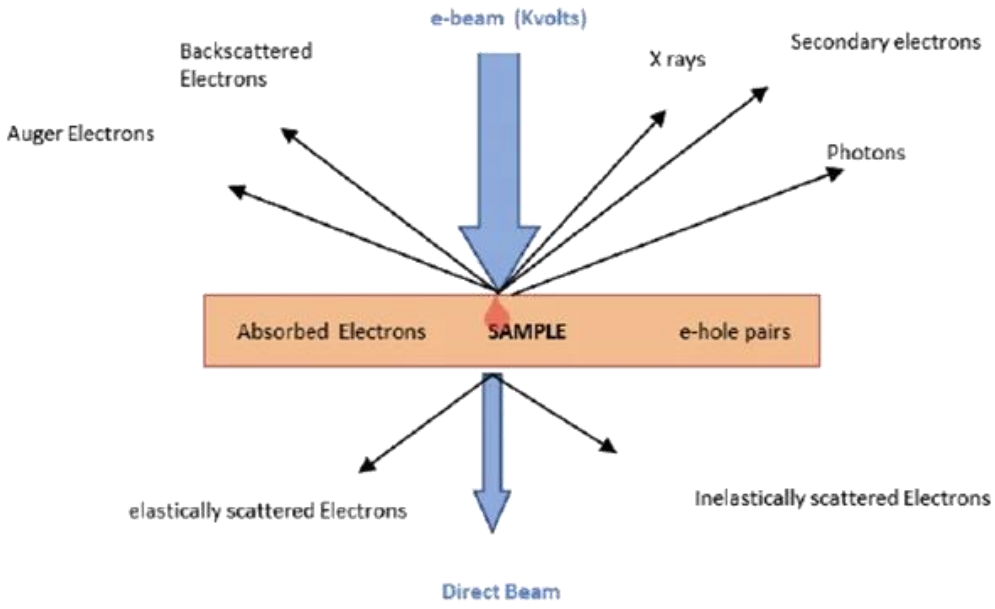

Figure 9: Scattering of electrons on interaction with matter

For membrane morphology, Scanning Electron Microscopy is used. It can also be used to examine the membrane's pores, both in terms of their number and distribution. As a result of the use of an electron gun and accelerating voltage, fast-moving electrons can be generated and sent down a column through numerous lenses and apertures. The sample is hit by an electron beam that is narrowly focused by the lenses and apertures. It's time to get that sample in there! To focus the electrons on the sample, both the column and the sample chamber must be under vacuum, which can be achieved by a series of pumps. Using scan coils located directly above the objective lens, the beam is focused on a specific area of the material. To learn more about a specific area of the sample, we can use the scanning electron beam. This process generates a variety of signals, which are then picked up and analyzed by the appropriate detectors. The Scanning Electron Microscope (SEM) consists of the following:

- Electron source
- Column and electromagnetic lenses
- Electron detector
- Sample chamber
- Display screen

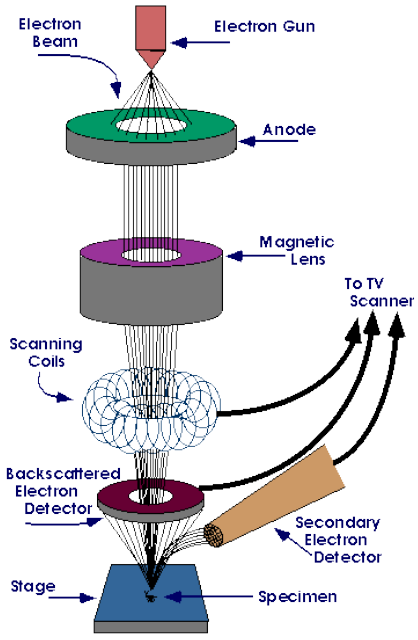

Figure 10: Schematic diagram of Scanning Electron Microscope

Membrane samples are analyzed using TESCAN MAIA3 Field Emission Scanning Electron Microscopy (FESEM) to determine their morphological properties. PET/MSNS films with filler-to-polymer ratios of 0.0025% to 0.2% (filler-to-polymer ratio) were used to characterize the distribution and structure of the pores in the membranes. To get the best results, the analysis is done at an accelerating voltage of 2 kV and magnifications that range from 10,000x to 25,000x. For this purpose, surface features were studied using SEM images that had just been taken at the end.

3.5.3. Permeation Testing System's working mechanism

In a gas permeation test system, the gas permeability through the membrane is determined. Permeability quantifies a fluid's ability to pass through a porous medium. P is defined as follows:

$$P = J\frac{\Delta l}{\Delta P}$$

, where P is the permeability co-efficient of the gas through the membrane.

J=(volumetric flow rate)/(area of membrane) is known as the fluid's volumetric flux.

l=The membrane's thickness

P = difference in pressure across the membrane

Additionally, the permeation of different gases through the same membrane can be utilized to determine the selectivity of one gas over another. The following formula determines the selectivity AB of gas A over gas B:

α_AB= P_A/P_B

For testing single gas permeation, a stainless steel gas permeation apparatus is utilized. The gas permeation apparatus is used to test the gas permeability of a membrane. Membrane cells are fitted with membranes. The feed gas is introduced at the top of the cell, while the permeate is discharged at the bottom. To determine the flow rate of permeate gas, a portion of the gas is passed through a bubble flow meter, where the time it takes for a fixed volume of bubbles to flow provides the gas flow rate. The diagram of the gas permeation apparatus is shown in (Figure 3.6).

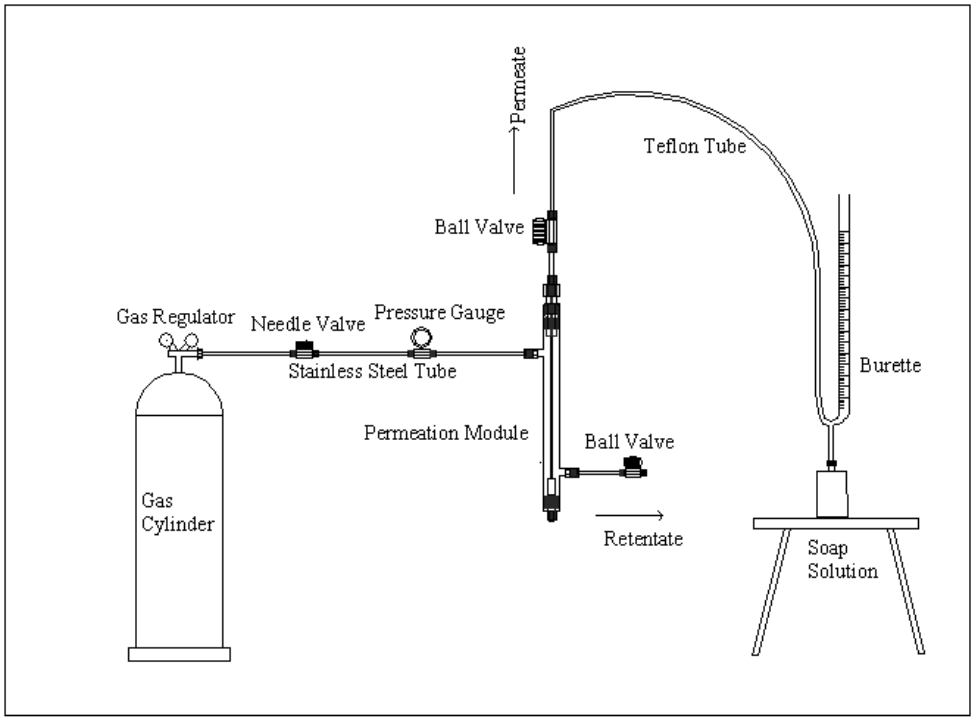

Figure 11: Schematic diagram of gas permeability testing system

We utilized the PHILOS Gas Permeability Test System, which contains a stainless-steel gas permeation rig, for testing single gas permeability. At 3 bar gauge pressure, the permeation of CO2 and O2 gases through the films was examined.

3.5.4. XRD's operating principle

One of the most commonly used methods for determining crystal structure is X-Ray Diffraction (XRD). Diffraction of X-Rays can also be used to determine the distance between atoms and the layers of atoms above and below them. A cathode ray tube, also known as a cathode ray generator, is used to generate x-rays, which are then filtered to produce monochromatic x-rays. The radiation is focused on a specific sample using a collimator, a device component. These X-Rays interact with the sample to produce the phenomenon of interference. Diffraction results in the collection of X-Rays, which can then be used to gain a wealth of information about the sample.

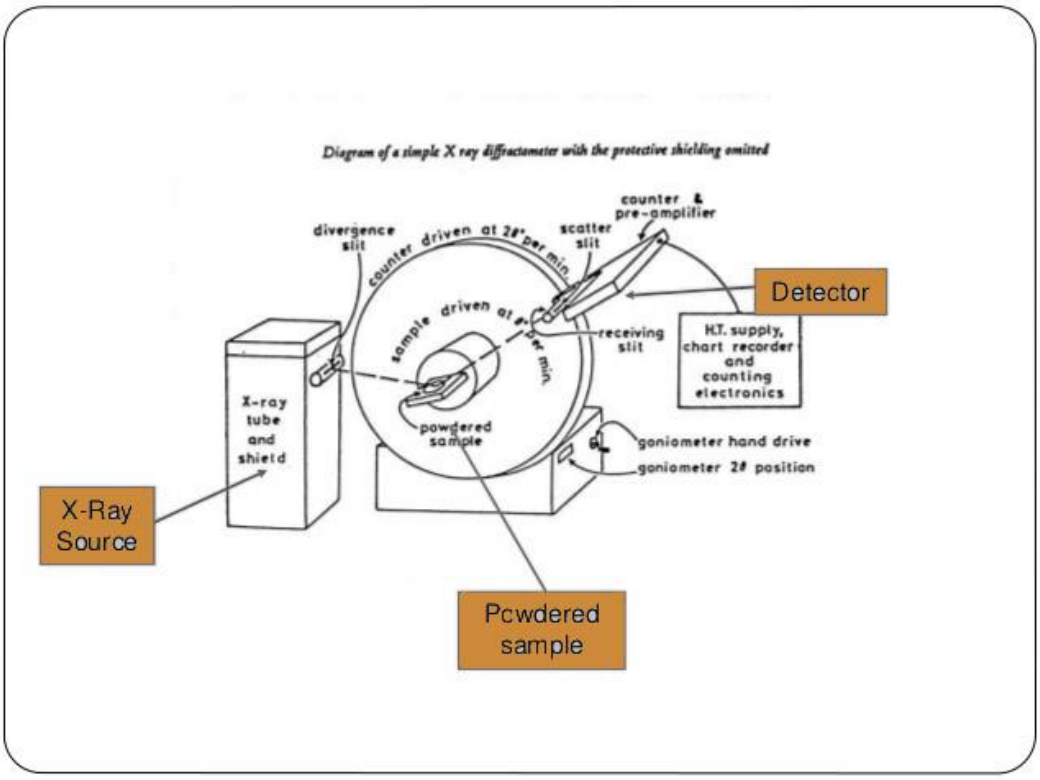

Figure 12: Schematic diagram of XRD

3.5.5. AFM's operating principle

An AFM scans a sample's surface using a cantilever with a razor-sharp tip. Toward the surface, the cantilever is deflected by the close-range, attractive force between the tip and surface. Cantilever deflection occurs when increasing repulsive force takes over as the cantilever is brought closer and closer to contact with the surface.

Detection of cantilever deflections is done using a laser beam. Any cantilever deflection causes slight changes in the direction of the reflected beam by reflecting an incident beam off the flat top of the cantilever. These changes can be tracked using a position-sensitive photo diode (PSPD). When an AFM tip passes over a raised surface feature, the PSPD records the cantilever deflection and the subsequent change in the beam direction.

Scanning the cantilever over an area of interest allows an AFM to capture images of the surface topography of a sample. The PSPD measures the deflection of the cantilever as a

result of the raised and lowered features on the sample surface. As long as the laser is kept in a fixed position using a feedback loop, an AFM can produce an accurate topographic map of the surface.

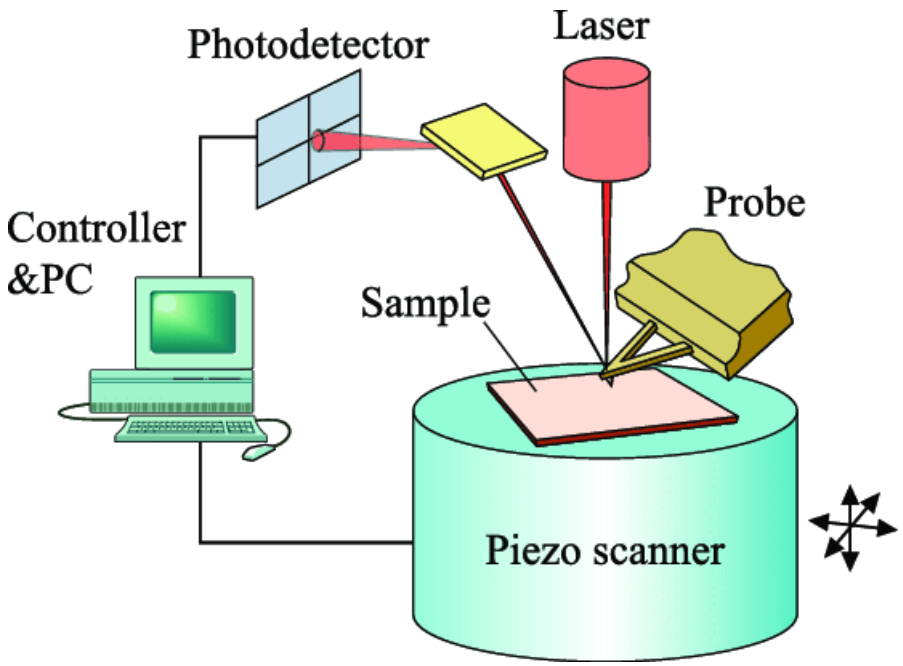

Figure 13: Schematic diagram of AFM

Chapter 4 - Results & Discussions

Through SEM and AFM, the dimensions of MSNS were characterized. SEM was used to evaluate the morphology of nanocomposites, and XRD was used to observe the structure of MSNS and the sort of interaction between MSNS and PET.

4.1. Permeation Models

A single gas permeation test was performed on all polymer nanocomposite films that contained MSNS in weight concentrations of 0.0025 percent, 0.005%, 0.01%, 0.02%, 0.03%, and 0.04%. The permeation testing was done in the PHILOS Gas Permeability Testing System with a gas permeation rig attached to the system. At a pressure of 3 bar, CO2 permeability through the films was calculated. The permeation results for CO2 are plotted in (Figure 4.1). There was zero selectivity for all samples.

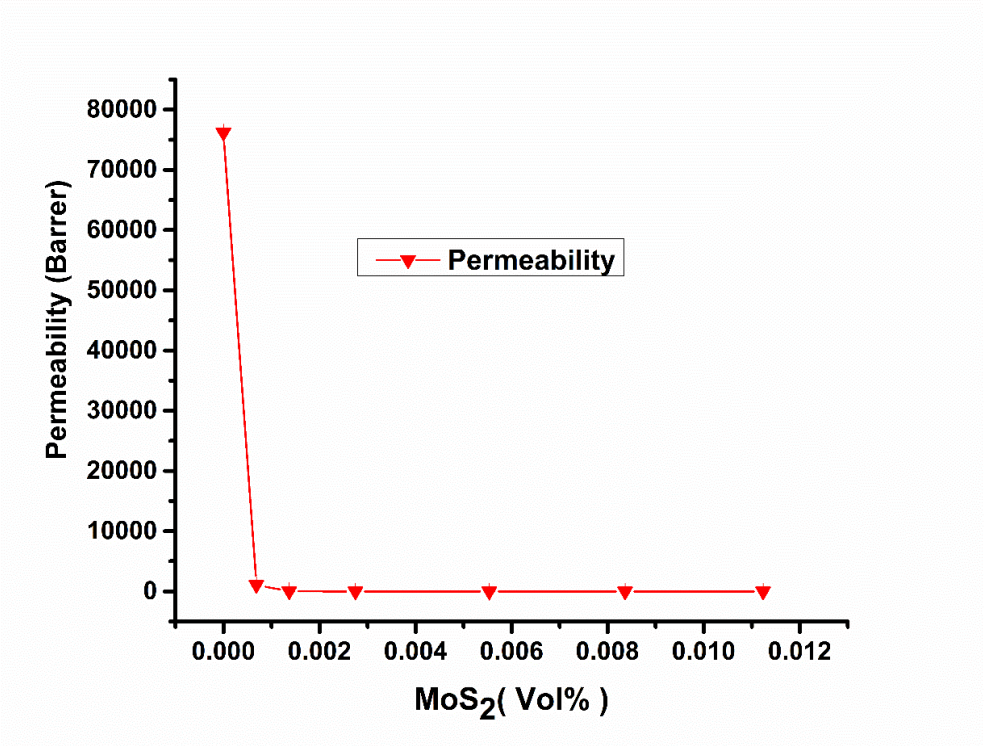

Figure 14: Effect of volume fraction of filler on permeability

71702.94724 Barrer permeation was found in a zero-loading sample film, while only 10083.22696 permeation was found in the 0.0025% sample, an 85.93 percent reduction in permeation. With each increase in filler loading, the amount of permeation decreased until it was zero for 12 hours at 0.01, 0.02, 0.03, and 0.04 percent, and no permeation for gas was observed at any of these concentrations. Of course, the results would have been different if the films had been tested for a longer period. Permeation data, on the other hand, provides a clear picture of how effective MSNS is at reducing the polymer's permeation. Even .01 percent had a semi-porous structure that showed no gas permeation for 12 hours, so samples ranging from.02 to.045 percent were prepared. The permeation results (Table 3) are also included.

Table 3: Experimental Permeation Results

Amount of Filler	Pressure (cm Hg)	Permeation (Barrer)	%Reduction in Permeation
.0025%	262.52	71703.22037	0
.005%	262.52	10083.26536	85.9375
.01%	262.52	41.30105493	99.9424
.02%	262.52	0	100
.03%	262.52	0	100
.04%	262.52	0	100

4.2. Permeation Models

The predictions of the model were based on an aspect ratio of 3000. From the curve fittings, we can tell that the Cussler model is close to the experimental values. The reason could be that the Cussler model takes into account that aspect ratio and volume fraction have a bigger effect on tortuosity and, as a result, lessen permeation than other models. For the highest loading composite, Cussler's model predicts that permeation will drop 8 times more than Nielsen's model. Different S values were also tried out with the Bhardwaj model. The Gusev and Lusti model was also used to figure out the current numbers, and the results were similar to Nielsen's. Comparisons of models with this work have been shown in (Figure 4.2). It was clear that the reduction in permeation that could be seen in experiments was more than what the theoretical models had predicted. Permeation tests were done for 12 hours for CO2. Since the films were not selective, CO2 results were plotted, but they can also be used for O2. Because the models don't take time into account, the results of experiments end up being bigger than what the models predicted.

4.2.1. Nielsen Model

Nielsen's model looks at how the volume fraction and aspect ratio affects the picture. It is assumed that the nanofiller is perpendicular to the flow of the gas and that their spread is uniform. The requirements for this model application are 10% and 1. Based on the dimensional analysis of MSNS, the aspect ratio is taken to be 3000. Figure 4.2 shows that the experimental values are very different from what the Nielsen model says they should be. This is because the criteria ($\alpha\emptyset \ll 1$) are not met according to (Table 4)

$$\frac{Kcomposite}{Kmatrix} = \frac{1-\emptyset}{1+\frac{\alpha}{2}\emptyset} \tag{4.1}$$

Table 4: Nielson Model Variables

Wt%	Vol% (∅)	Aspect Ratio (α)	Relative Permeability (theoretical)	Permeability (Barrer)	Relative Permeability (Experimental)	Criteria $\alpha\emptyset \ll 1$
0	0	3000	1	71702.94724	1	0
.0025%	0.000683	3000	0.493589744	10083.22696	0.140625	2.049
.005%	0.001369	3000	0.327106993	41.30089761	0.000576	4.107
.01%	0.002747	3000	0.194742489	0	0	8.241
.02%	0.005535	3000	0.106902023	0	0	16.605
.03%	0.008364	3000	0.073202525	0	0	25.092
.04%	0.011236	3000	0.055380743	0	0	33.708

4.2.2. Cussler Model

Cussler's model assumes that the nanofillers inside the polymer matrix are evenly spread out and that the orientation of the nanofillers is parallel to the flow. 3000 was chosen as the aspect ratio. The model is most useful for lower loadings, and the criteria are $\emptyset \ll 1\,\% \,\&\, \alpha\emptyset \gg 1$. As you can see in Table 5, the criterion is met, which means that the Cussler model is close to what we found in our experiments.

$$\frac{Kcomposite}{Kmatrix} = \left(1 + \frac{\alpha^2\emptyset^2}{1-\emptyset}\right)^{-1} \tag{4.2}$$

Table 5: Cussler Model Variables

Wt.%	Vol% (∅)	Aspect Ratio (α)	Relative Permeability (theoretical)	Permeability (Barrer)	Relative Permeability (Experimental)	Criteria α∅ ≫ 1
0	0	3000	1	71702.94724	1	0
.0025%	0.000683	3000	0.192233378	10083.22696	0.140625	2.049
.005%	0.001369	3000	0.055925218	41.30089761	0.000576	4.107
.01%	0.002747	3000	0.01446891	0	0	8.241
.02%	0.005535	3000	0.003593681	0	0	16.605
.03%	0.008364	3000	0.00157241	0	0	25.092
.04%	0.011236	3000	0.000869466	0	0	33.708

4.2.3. Bharadwaj Model

This model looks at how the direction of nanofillers affects permeation. It uses the S factor. When the orientation is perpendicular, S = 1, and the model becomes the Nielsen model as in figure 4.2. Again, 3000 was chosen as the aspect ratio. Using the Bharadwaj model, it is also possible to predict orientation.

$$\frac{Kcomposite}{Kmatrix} = \frac{1-\emptyset}{1+\frac{L}{2W}\emptyset\frac{2}{3}\left(S+\frac{1}{2}\right)} \tag{4.3}$$

$$S=\frac{1}{2}(3\cos^2\Theta-1) \tag{4.4}$$

4.2.4 Gusev and Lusti Model:

The model works for the random scattering of discs that don't touch each other. Picard et al. used the coefficient values β =0.71 and xo=3.47 to get results for nylon-6/montmorillonite composites that were similar to those from the Nielsen model [70]. For this prediction, the same values were used. 3000 was thought to be the aspect ratio.

$$\frac{Kcomposite}{Kmatrix} = \exp\left[-\left(\frac{\alpha\emptyset}{xo}\right)^{\beta}\right] \quad (4.5)$$

Table 6: Gusev & Lusti Model Variables

Wt.%	Vol% ($\emptyset$)	Aspect Ratio (α)	Relative Permeability (theoretical)	Permeability (Barrer)	Relative Permeability (Experimental)
0	0	3000	1	71702.94724	1
.0025%	0.000683	3000	0.502581	10083.22696	0.140625
.005%	0.001369	3000	0.32404	41.30089761	0.000576
.01%	0.002747	3000	0.157526	0	0
.02%	0.005535	3000	0.04788	0	0
.03%	0.008364	3000	0.017005	0	0
.04%	0.011236	3000	0.006578	0	0

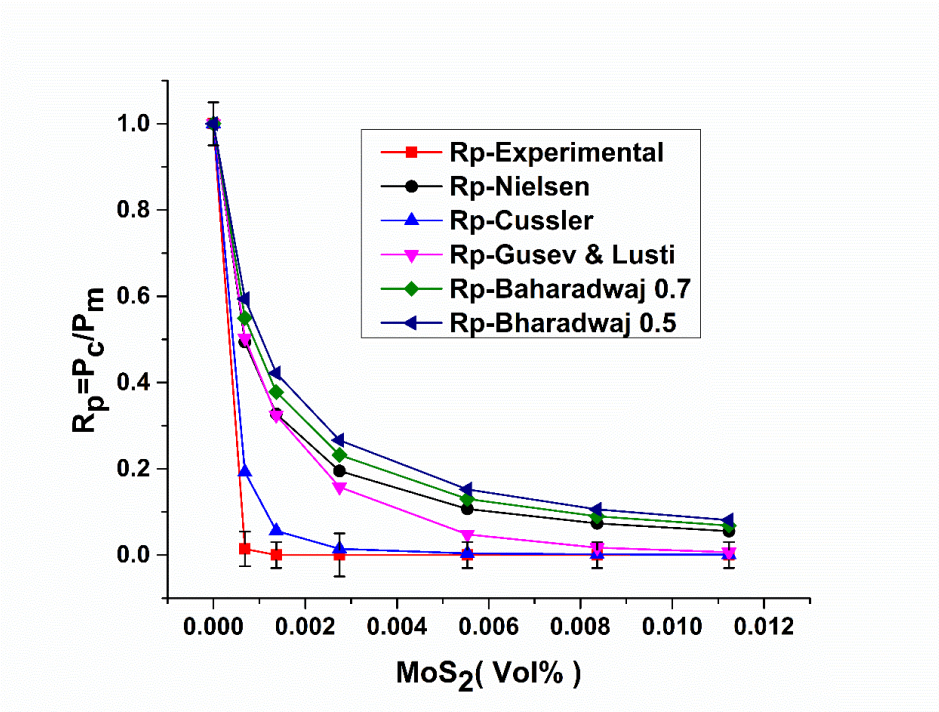

Figure 15: Nielsen, Cussler, Bharadwaj, Gusev, and Lusti Models combined comparison with experimental permeation results

4.3. Analytical Measurement of MNNS

Nanosheets were analyzed for their dimensions through AFM and SEM. Figure 16 shows the bulk MoS_2 powder SEM images taken at 20,000 and 30,000 magnifications which specifies that they are non-exfoliated at this stage. A stack-like structure is observable. In comparison with figure 4.4, it can be seen that a Few layers of MSNS are exfoliated successfully. SEM images of MSNS are taken at the same magnifications as bulk to check the conversion of bulk material into nanosheets.

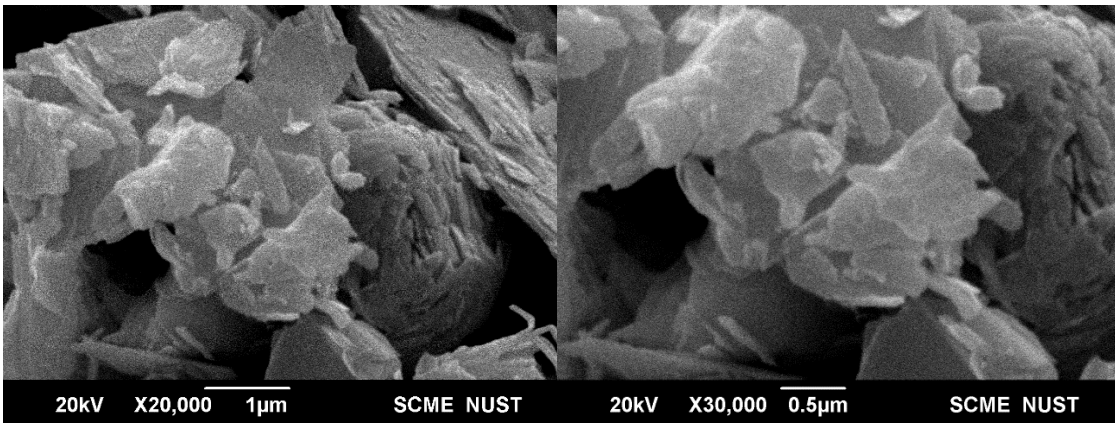

Figure 16: MoS_2 bulk at 20,000 and 30,000 magnifications

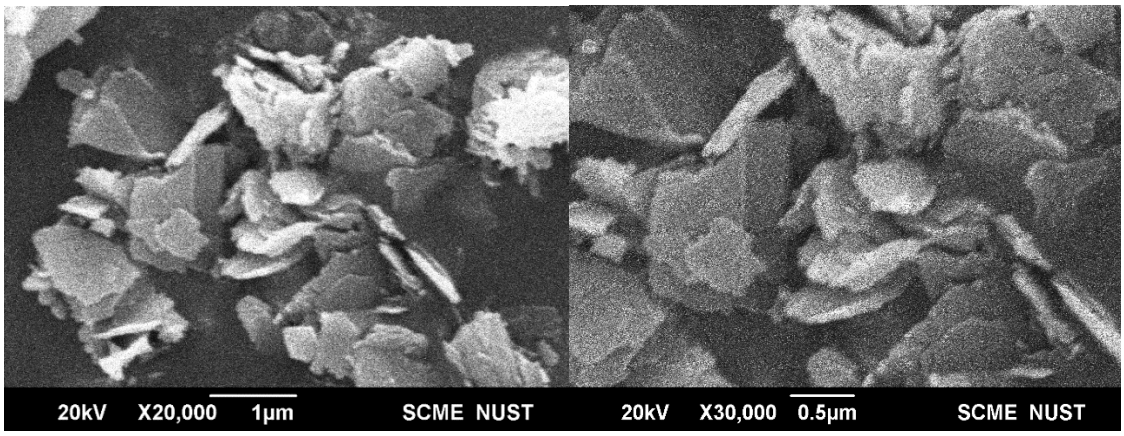

Figure 17: MoS_2 Nanosheets at 20,000 and 30,000 magnifications

The AFM histogram suggests that the average thickness of nanosheets is approximately 1.63 millimeters.

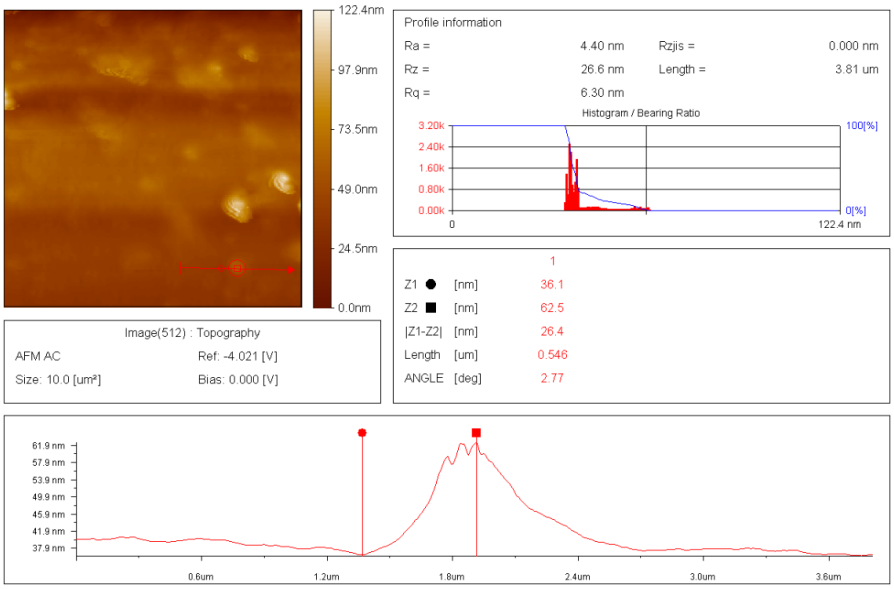

Figure 18: AFM histogram of MoS_2 Nanosheets

4.4. SEM

Film samples varied in their depiction of a porous upper surface and dense lower surface morphological pattern. Upon closer inspection, it was discovered that the top surface had a rough evaporation stature, while the bottom surface had shiny optics.

4.4.1. Top Surface

As the number of nanosheets increases, the shape of the material changes in a big way. Figure 4.6 shows that a pure PET film is completely porous. Figures 19–21 show that the porosity decreases as the weight percent of nanosheets go up. Compared to a pure PET film, the 0.0025wt percent composite has smaller pores and a more even distribution of pores, which shows that the nanosheets were successfully incorporated. The same pattern holds for all the higher concentration composites, with the 0.01wt percent composite having an almost perfect and uniform dense structure. When you think about how many nanosheets were used, it goes without saying that the changes in shape that samples with a high concentration of nanosheets show are very interesting. It should also be noted that

nanosheets are almost impossible to see on the surface. This could be because they are used so little.

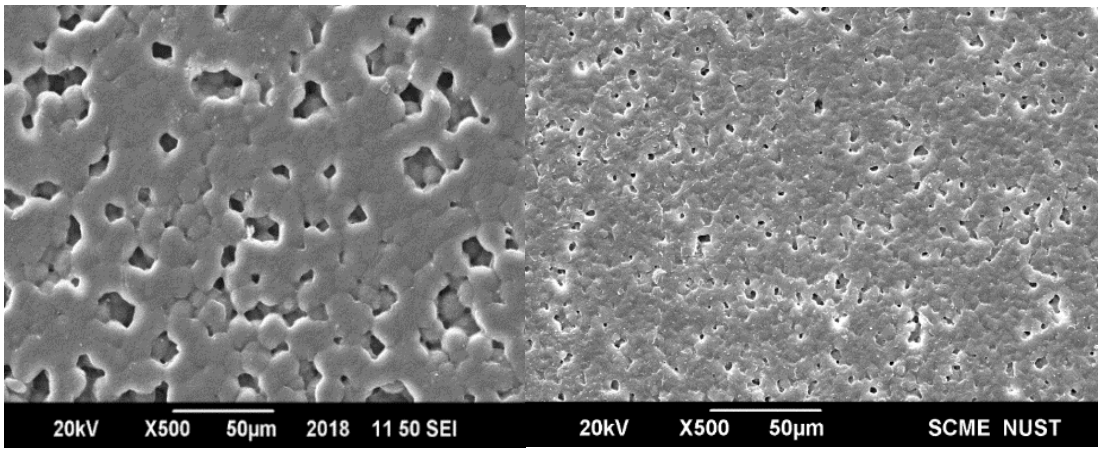

Figure 19: a) Pure PET film-Surface b) **.**0025wt%-Surface

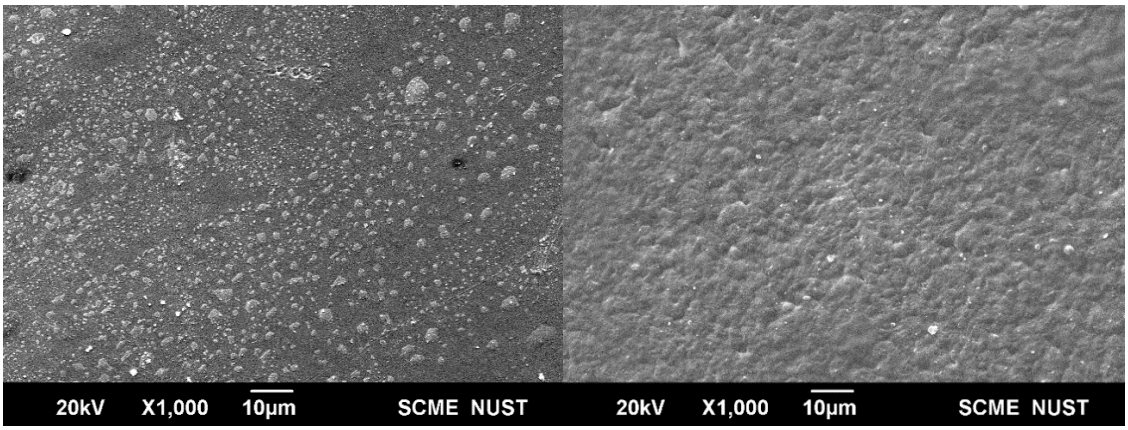

Figure 20: a).005wt%-Surface b).01wt%-Surface

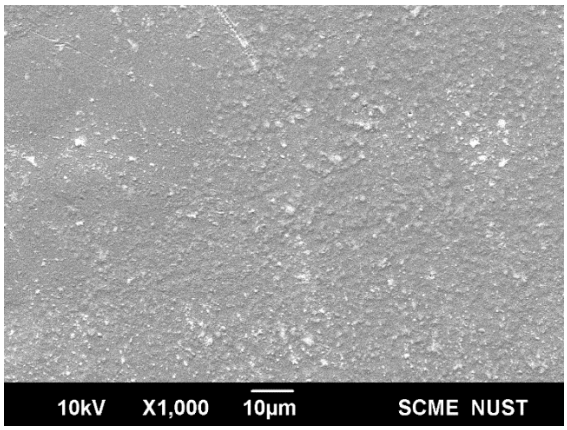

Figure 21: .02wt%-Surface

4.4.2 Cross-Section

SEM cross-section images were obtained that are immediately clear and self-explanatory (Figure 22-25). From top to bottom, we can see a change in the arrangement of polymeric chains in Pure film, and a similar pattern can be observed in higher-weight percent composites. A pure sample has a dense appearance with little spacing between chains, but from the middle to the top of the cross-section, chains appear to be slightly tangled, with large pores and voids, in the middle to the top portion. At 0.0025 parts per million, the material has a semi-dense structure. Underneath the 0.01 wt. percent sample shows a nearly perfect dense bottom structure. Drying of membrane fabrication leaves gaps that polymer fills to a large extent, but not completely, which is the reason for the appearance of pores in the pure sample.

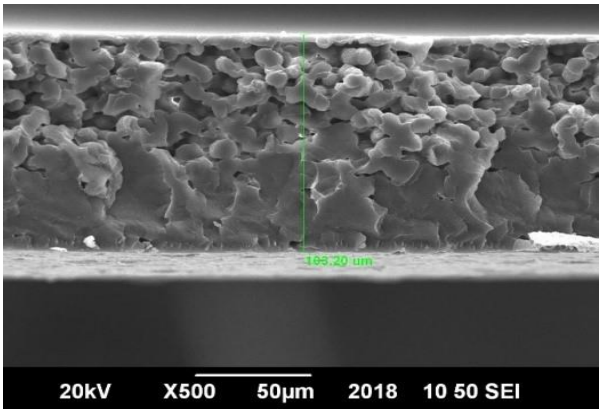

Figure 22: Pure-Cross-Section

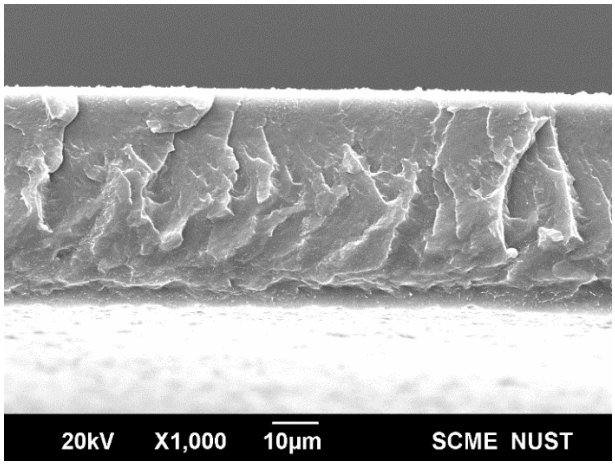

Figure 23: .0025wt%-Cross-Section

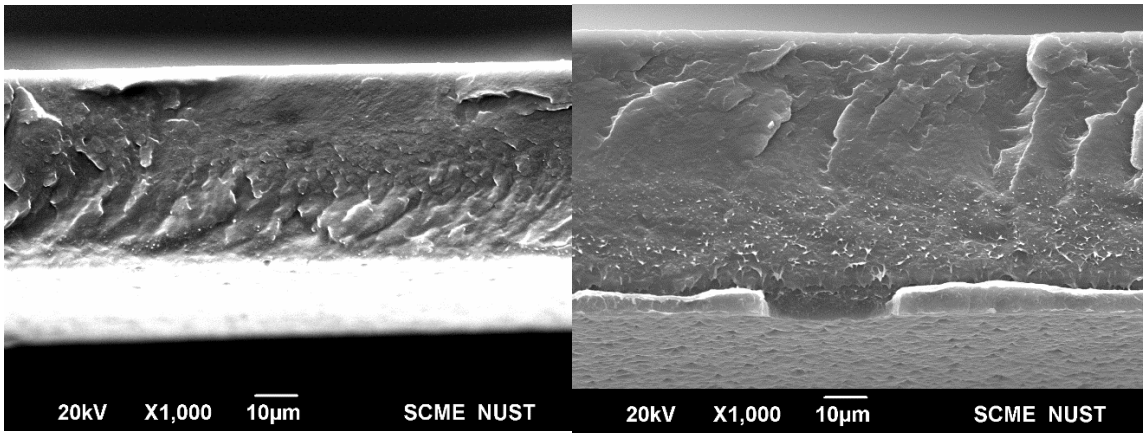

Figure 24: a).005wt%-Cross-Section b) .01wt%-Cross-Section

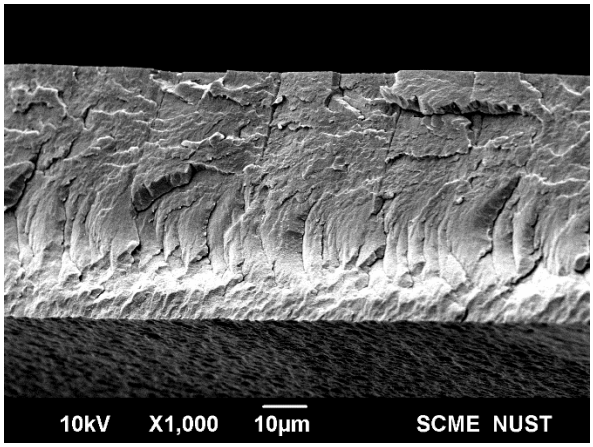

Figure 25: .02wt%-Cross-Section

But in composites, the gaps in polymeric chains are mostly filled by the polymer itself and the remaining nanosheets, resulting in a dense structure after the solvent evaporates and leaves the gaps. In addition, because solvent evaporation is a slow process, most of the polymer settles at the bottom, resulting in a denser structure in the early stages.

4.4. XRD

4.4.1. XRD of nanosheets

The XRD pattern in Figure 26 (lower portion) reveals crystalline, single-phase MoS_2 nanosheets with a hexagonal crystal structure. No extra peaks were detected. For comparison with the standard XRD pattern of MoS_2 samples, bulk MoS_2 powder x-ray patterns have been provided. (JCPDS-37-1492) At 31.9◦, 39.69◦, and 49.51◦, corresponding to the (100), (103), and (105) planes, the characteristic peaks of MoS_2

nanosheets were observed. The abrupt decrease of (002) reflections and the broadness of peaks in comparison to bulk MoS_2 crystals specify that the resulting products are single-layer or few-layer MoS_2 [71].

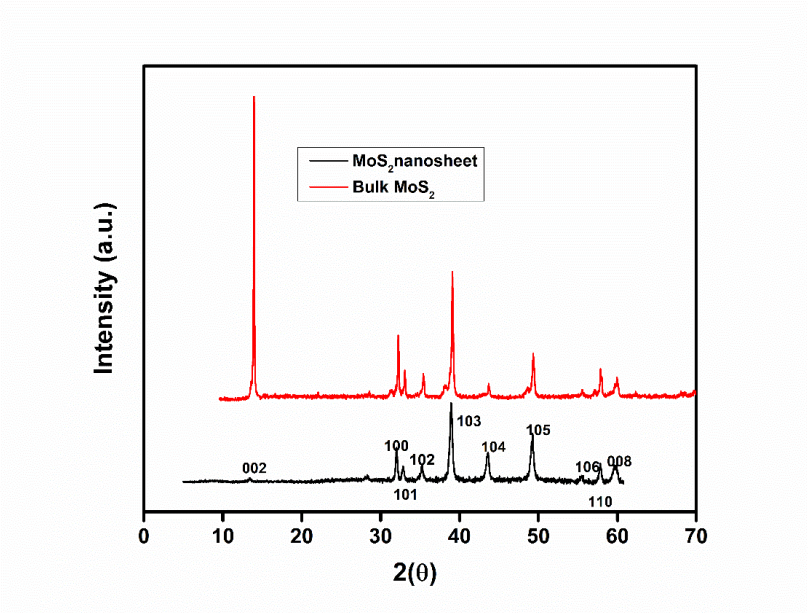

Figure 26: Comparison of XRD pattern of MoS2 bulk and MoS2 nanosheets

4.4.2. XRD of nanocomposites

Figure 27 shows the XRD pattern of PET polymer. No sharp peaks were detected here which confirms the polymeric behavior of the material.

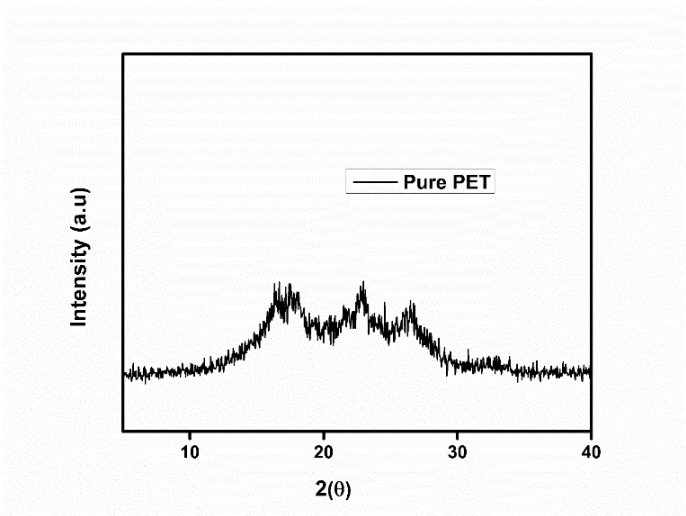

Figure 27: XRD pattern of Pure PET

In comparison with figure 4.3, the nanocomposite shows some crystallinity peaks with the addition of fillers.

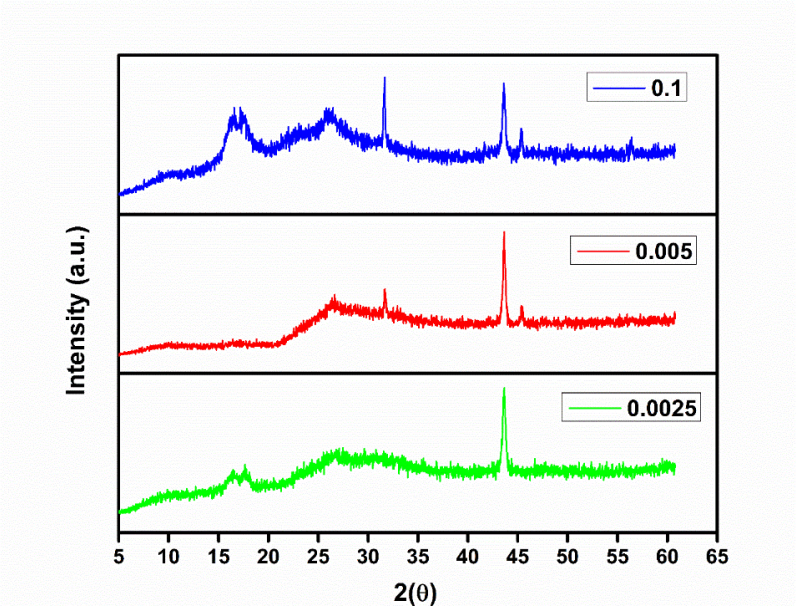

Figure 28: PET/MSNS nanocomposites XRD

Samples were found to retain their crystal structure to varying degrees based on the presence of peaks at 31.3 and 43.9. Peaks in PET films with no filler loading had the lowest peak intensities because heat treatment at high temperatures loosens the polymer chain. In addition to the SEM results, all composites show an increase in crystallinity (Figure 28), which confirms the role of nanosheets in increasing chain entanglement and thus increasing crystallinity and decreasing permeation. Each sample's XRD and SEM results are in agreement with each other. h-interaction MoS_2 with polymer was found to be strictly physical, as no peak shift was observed for any of the composites tested.

Conclusion

PET/MoS_2 nanocomposites were synthesized by using a novel and easy-to-use method, solution processing. Because of good dispersion, nanocomposites showed enhanced gas barrier properties at low loadings, compared to theoretical models, and the experimental results closely resembled the Cussler model and showed higher reductions, which is because the permeation was performed for 12 hours only, experimental results would comply much better with theoretical models with prolonged permeation testing... In addition, a theoretical model that takes into account time must also be developed. CO2 permeation was reduced by 99% with a sample concentration of just.005wt percent. For composites, the SEM results confirmed the permeation results by revealing a dense surface. The webbed structure formed by MSNS was also found to be responsible for the increased elongation-at-break that was observed. In addition to the SEM results, all composites show an increase in crystallinity (Figure 4.18), which confirms the role of nanosheets in increasing chain entanglement and thus increasing crystallinity and decreasing permeation.

Future Recommendations

Parameters of experimentations such as RPM of centrifugation during nanosheet synthesis and weight percentage of filler in polymer PET can be varied and studied in the future. RPM has a direct effect on the size of nanosheets. Higher values of RPM can give us nanosheets having a small size which can be used in other applications apart from corrosion. Nanosheets have a great scope in other branches of science i.e., biomedical, catalytic activities, and hydrogen production so other problems of industries can be sorted out. Furthermore, the high-scale fabrication of nanosheets will be a very remarkable achievement. Research on increasing the yield of nanosheets could also be done. The gas barrier properties of PET-MSNS films were evaluated for twelve hours, and results were compared to theoretical predictions, with the reduction in permeation in experiments exceeding the models' predicted values. It is suggested that a permeation model with time as a variable be developed to obtain more precise results.

References

[1]. Ali, M.M., et al., *Corrosion protection of steel pipelines with metal-polymer composite barrier liners.* 2020. **81**: p. 103407.

[2]. Wasiu, A.B. and M.R. Heikal, *The effect of carbon dioxide content-natural gas on the performance characteristics of engines: a review*. 2012.

[3]. Zahid, M., et al., *Graphene morphology effect on the gas barrier, mechanical and thermal properties of thermoplastic polyurethane.* 2020. **200**: p. 108461.

[4]. Zhang, J., et al., *2D nanomaterials for tissue engineering application.* 2020. **13**(8): p. 2019-2034.

[5]. Murali, A., et al., *Emerging 2D nanomaterials for biomedical applications.* 2021. **50**: p. 276-302.

[6]. Tiwari, S.K., et al., *Graphene research and their outputs: Status and prospect.* 2020. **5**(1): p. 10-29.

[7]. Telkhozhayeva, M., et al., *Higher Ultrasonic Frequency Liquid Phase Exfoliation Leads to Larger and Monolayer to Few-Layer Flakes of 2D Layered Materials.* 2021. **37**(15): p. 4504-4514.

[8]. Rex, W.J. and D.J. Tennant, *Polymeric linear terephthalic esters*. 1949, Google Patents.

[9]. Wyeth, N. and R. Roseveare, *Biaxially oriented poly (ethylene terephthalate) bottle*. 1973, Google Patents.

[10]. MacArthur, D.E., D. Waughray, and M.R. Stuchtey. *The new plastics economy, rethinking the future of plastics*. in *World Economic Forum*. 2016.

[11]. Boutroy, N., et al., *Hydrogenated amorphous carbon film coating of PET bottles for gas diffusion barriers.* 2006. **15**(4-8): p. 921-927.

[12]. Kuzminova, A., et al. *Barrier coatings on polymeric foils for food packaging*. in *WDS*. 2013.

[13]. Nakaya, M., A. Uedono, and A.J.C. Hotta, *Recent progress in gas barrier thin film coatings on PET bottles in food and beverage applications.* 2015. **5**(4): p. 987-1001.

[14]. Munoz, N., *Using Oxygen and Biopreservation as Hurdles to Improve Safety of Cooked Food during Storage at Refrigeration Temperatures*. 2018: Washington State University.

[15]. Beeva, D., et al., *Controlling the barrier properties of polyethylene terephthalate. A review.* 2015. **42**(7): p. 45-52.

[16]. Profaizer, M. *Passive Barrier Assessment of PET Bottles through an FEM Simulation of Gas Permeability*. in *Excerpt from the Proceedings of the COMSOL Multiphysics User's Conference*. 2005. Citeseer.

[17]. Nakaya, M., et al., *Gas and flavor barrier thin film coating to plastic closures.* 2018. **4**(1): p. 1-17.

[18]. Naz, R., *Storage in polyethylene terephthalate bottles: changes and shelf life*, in *Fruit Juices*. 2018, Elsevier. p. 621-635.

[19]. Sharma, M.D., C. Mahala, and M.J.C. Basu, *AgPd alloy nanoparticles decorated MoS_2 2D nanosheets: efficient hydrogen evolution catalyst in wide pH condition.* 2019. **4**(1): p. 378-386.

[20]. Zhao, H., et al., *Structural defects in 2D MoS_2 nanosheets and their roles in the adsorption of airborne elemental mercury.* 2019. **366**: p. 240-249.

[21]. Li, Y., et al., *2D/2D/2D heterojunction of Ti3C2 MXene/MoS_2 nanosheets/TiO2 nanosheets with exposed (001) facets toward enhanced photocatalytic hydrogen production activity.* 2019. **246**: p. 12-20.

[22]. Liu, H., et al., *Boosting zinc-ion intercalation in hydrated MoS_2 nanosheets toward substantially improved performance.* 2021. **35**: p. 731-738.

[23]. Kanaujiya, N., et al., *CoMn2O4 nanoparticles decorated on 2D MoS_2 frame: a synergetic energy storage composite material for practical supercapacitor applications.* 2021. **35**: p. 102302.

[24]. Kasinathan, K., et al., *Cyclodextrin functionalized multi-layered MoS_2 nanosheets and its biocidal activity against pathogenic bacteria and MCF-7 breast cancer cells: Synthesis, characterization and in-vitro biomedical evaluation.* 2021. **323**: p. 114631.

[25]. Abinaya, R., et al., *Enhanced thermoelectric figure-of-merit of MoS_2/α-MoO3 nanosheets via tuning of sulphur vacancies.* 2021. **416**: p. 128484.

[26]. Xu, X., et al., *An excellent triethylamine (TEA) sensor based on unique hierarchical MoS2/ZnO composites composed of porous microspheres and nanosheets.* 2021. **333**: p. 129616.

[27]. Liu, M.-C., et al., *Large interlayer spacing 2D Ta4C3 matrix supported 2D MoS_2 nanosheets: A 3D heterostructure composite towards high-performance sodium ions storage.* 2021. **169**: p. 573-581.

[28]. Jlidi, Z., et al., *Temperature effect on structural, morphological and optical properties of 2D-MoS2 layers: An experimental and theoretical study.* 2021. **228**: p. 166166.

[29]. Rahman, R., et al., *Tuning of structural and optical properties with enhanced catalytic activity in chemically synthesized Co-doped MoS_2 nanosheets.* 2021. **11**(3): p. 1303-1319.

[30]. Xiao, Y., et al., *Ethylenediamine-assisted phase engineering of 1T/2H–MoS_2/graphene for efficient and stable electrocatalytic hydrogen evolution.* 2021. **46**(21): p. 11688-11700.

[31]. Yu, H., et al., *Freestanding nanosheets of 1T-2H hybrid MoS_2 as electrodes for efficient sodium storage.* 2021. **67**: p. 237-242.

[32]. Zhou, P., et al., *Hydrothermal synthesis of novel ternary hierarchical MoS_2/TiO2/clinoptilolite nanocomposites with remarkably enhanced visible light response towards xanthates.* 2021. **542**: p. 148578.

[33]. Luo, X., et al., *One-pot hydrothermal synthesis of MoS_2 anchored corncob-derived carbon nanospheres for use as a high-capacity anode for reversible Li-ion battery.* 2021. **296**: p. 122020.

[34]. Liu, Z., et al., *Self-assembled MoS_2/3D worm-like expanded graphite hybrids for high-efficiency microwave absorption.* 2021. **174**: p. 59-69.

[35]. Ikram, M., et al., *Outstanding performance of silver-decorated MoS2 nanopetals used as nanocatalyst for synthetic dye degradation.* 2020. **124**: p. 114246.

[36]. Huang, Y., et al., *Synthesis and photocatalytic performance of MoS2/Polycrystalline black phosphorus heterojunction composite.* 2021. **46**(5): p. 3530-3538.

[37]. Liu, Y., et al., *Role of structural characteristics of MoS2 nanosheets on Pb2+ removal in aqueous solution.* 2021. **22**: p. 101385.

[38]. Arefi-Oskoui, S., et al., *Toxicity evaluation of bulk and nanosheet MoS2 catalysts using battery bioassays.* 2021. **268**: p. 128822.

[39]. Zhang, M., et al., *Visible light-induced antibacterial effect of MoS2: Effect of the synthesis methods.* 2021. **411**: p. 128517.

[40]. Zribi, R., et al., *Exfoliated 2D-MoS2 nanosheets on carbon and gold screen printed electrodes for enzyme-free electrochemical sensing of tyrosine.* 2020. **303**: p. 127229.

[41]. Singh, J., et al., *Cost-effective scalable synthesis of few layers MoS2 based thin film for sunlight enforced photocatalytic activity.* 2020. **110**: p. 110506.

[42]. Zribi, R., et al., *Simultaneous and selective determination of dopamine and tyrosine in the presence of uric acid with 2D-MoS2 nanosheets modified screen-printed carbon electrodes.* 2020. **24**: p. 100187.

[43]. Kaushik, S., et al., *Study of sonication assisted synthesis of molybdenum disulfide (MoS2) nanosheets.* 2020. **21**: p. 1969-1975.

[44]. Karmakar, S., et al., *Synthesis of bilayer MoS2 nanosheets by green chemistry approach and its application in triboelectric and catalytic energy harvesting.* 2020. **844**: p. 155690.

[45]. Roy, S., et al., *Mechanistic insight into the antibacterial activity of chitosan exfoliated MoS2 nanosheets: membrane damage, metabolic inactivation, and oxidative stress.* 2019. **2**(7): p. 2738-2755.

[46]. Rahimi, K., et al., *Enhancement of sunlight-induced photocatalytic activity of ZnO nanorods by few-layer MoS2 nanosheets.* 2019. **234**: p. 134-137.

[47]. Yao, Y., et al., *High-concentration aqueous dispersions of MoS2.* 2013. **23**(28): p. 3577-3583.

[48]. Ma, L., et al., *PtNi bimetallic nanoparticles loaded MoS2 nanosheets: Preparation and electrochemical sensing application for the detection of dopamine and uric acid.* 2019. **1055**: p. 17-25.

[49]. Wu, P.-R., Z. Liu, and Z.-L.J.A.o. Cheng, *Ultrasound-Assisted Alkaline Solution Reflux for As-Exfoliated MoS2 Nanosheets.* 2019. **4**(6): p. 9823-9827.

[50]. Santalucia, R., et al., *Few-layered MoS2 nanoparticles covering anatase TiO2 nanosheets: Comparison between ex situ and in situ synthesis approaches.* 2020. **11**(1): p. 143.

[51]. Li, H., et al., *Efficient visible light driven ammonia synthesis on sandwich structured C3N4/MoS2/Mn3O4 catalyst.* 2021. **281**: p. 119476.

[52]. Xu, W., et al., *Molybdenum disulfide (MoS2) nanosheets-based hydrogels with light-triggered self-healing property for flexible sensors.* 2021. **586**: p. 601-612.

[53]. Chen, W., et al., *Solid-state synthesis of ultrathin MoS2 as a cocatalyst on mesoporous g-C3N4 for excellent enhancement of visible light photoactivity.* 2020. **836**: p. 155401.

[54]. Yuan, Y.-J., et al., *Liquid exfoliation of g-C3N4 nanosheets to construct 2D-2D MoS2/g-C3N4 photocatalyst for enhanced photocatalytic H2 production activity.* 2019. **246**: p. 120-128.

[55]. Alomar, M., et al., *Controlling the growth of ultrathin MoS2 nanosheets/CdS nanoparticles by two-step solvothermal synthesis for enhancing photocatalytic activities under visible light.* 2019. **480**: p. 1078-1088.

[56]. Wu, W., et al., *High throughput synthesis of defect-rich MoS2 nanosheets via facile electrochemical exfoliation for fast high-performance lithium storage.* 2019. **542**: p. 263-268.

[57]. Hamzehlou, S. and A. Katbab, *Bottle-to-bottle recycling of PET via nanostructure formation by melt intercalation in twin screw compounder: Improved thermal, barrier, and microbiological properties.* Journal of applied polymer science, 2007. **106**(2): p. 1375-1382.

[58]. Frounchi, M. and A. Dourbash, *Oxygen barrier properties of poly (ethylene terephthalate) nanocomposite films.* J Macromolecular Materials Engineering, 2009. **294**(1): p. 68-74.

[59]. Labde, R.K., *Preparation and characterization of polyethylene terephthalate/montmorillonite nanocomposites by in-situ polymerization method*. 2010, University of Toledo.

[60]. Gunes, K., et al., *Fast in situ copolymerization of PET/PEN blends by ultrasonically-aided extrusion.* J Polymer, 2010. **51**(5): p. 1071-1081.

[61]. Donadi, S., et al., *PET/PA nanocomposite blends with improved gas barrier properties: Effect of processing conditions.* Journal of applied polymer science, 2011. **122**(5): p. 3290-3297.

[62]. Sanchez-Garcia, M., E. Gimenez, and J. Lagaron, *Novel PET nanocomposites of interest in food packaging applications and comparative barrier performance with biopolyester nanocomposites.* Journal of Plastic Film Sheeting, 2007. **23**(2): p. 133-148.

[63]. Wang, Y. and S.A. Jabarin, *Novel preparation method for enhancing nanoparticle dispersion and barrier properties of poly (ethylene terephthalate) and poly (m-xylylene adipamide).* Journal of applied polymer science, 2013. **129**(3): p. 1455-1465.

[64]. Cui, Y., et al., *Gas barrier properties of polymer/clay nanocomposites.* J RSC Advances, 2015. **5**(78): p. 63669-63690.

[65]. Shim, S.H., et al., *Facile method to functionalize graphene oxide and its application to poly (ethylene terephthalate)/graphene composite.* ACS applied materials interfaces, 2012. **4**(8): p. 4184-4191.

[66]. Al-Jabareen, A., et al., *Improving the oxygen barrier properties of polyethylene terephthalate by graphite nanoplatelets.* Journal of applied polymer science, 2013. **128**(3): p. 1534-1539.

[67]. Esmaeilzadeh, A., et al., *Preparation and Characterization of Layered Silicate Polyethylene Terephthalate Nanocomposite by in Situ Polymerization.* Journal of Petroleum Science and Technology, 2016. **6**(2): p. 45-55.

[68]. Szymczyk, A., et al., *Oxygen Barrier Properties and Melt Crystallization Behavior of Poly(ethylene terephthalate)/Graphene Oxide Nanocomposites.* Journal of Nanomaterials, 2015. **2015**: p. 10.

[69]. Lucchetta, G. and S.J.K.E.M. Chirico, *Acetaldehyde generation in processing PET by means of hot runner systems.* 2014.

[70]. Picard, E., et al., *Barrier properties of nylon 6-montmorillonite nanocomposite membranes prepared by melt blending: influence of the clay content and dispersion state: consequences on modelling.* 2007. **292**(1-2): p. 133-144.

[71]. Veeramalai, C.P., et al., *Enhanced field emission properties of molybdenum disulphide few layer nanosheets synthesized by hydrothermal method.* 2016. **389**: p. 1017-1022.